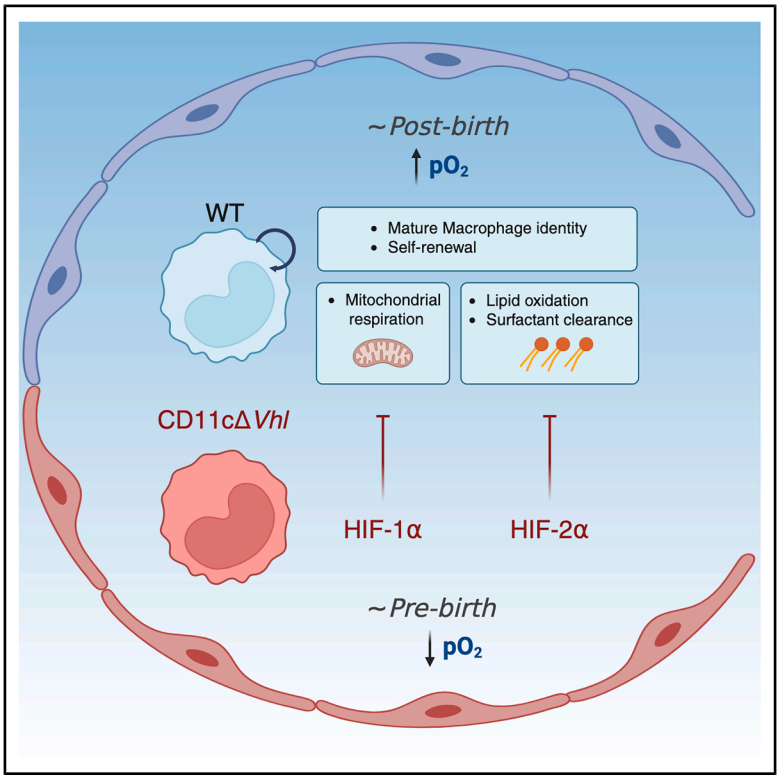
Cell Reports



# HIF-1α and HIF-2α differentially regulate alveolar macrophage maturation and function

## Graphical abstract




## Highlights

- HIF-1α drives the glycolytic reprogramming in pVHL-deficient alveolar macrophages
- Alveolar macrophage self-renewal is impaired by both HIF-1α and HIF-2α
- HIF-2α compromises surfactant clearance capacity in alveolar macrophages

## Authors

Elena Priego, Irene Adan-Barrientos, Ruth Conde-Garrosa, ..., Joaquín Amores-Iniesta, Helena M. Izquierdo, David Sancho

## Correspondence

helena.izquierdo-fernandez@curie.fr (H.M.I.), dsancho@cnic.es (D.S.)

## In brief

pVHL regulates alveolar macrophage phenotypical maturation and self-renewal. Priego et al. show that HIF-1α specifically drives a glycolytic switch and controls self-renewal along with HIF-2α, while HIF-2α specifically regulates lipid oxidation and surfactant clearance. This reveals how oxygen sensing shapes macrophage identity and adaptation to the alveolar niche.

Priego et al., 2026, Cell Reports *45*, 117447
June 23, 2026 © 2026 The Authors. Published by Elsevier Inc.
https://doi.org/10.1016/j.celrep.2026.117447

CellPress

Cell Reports

CellPress
OPEN ACCESS

Report

# HIF-1α and HIF-2α differentially regulate alveolar macrophage maturation and function

Elena Priego,[1,2,3,8] Irene Adan-Barrientos,[1,2,4,8] Ruth Conde-Garrosa,[1] Sarai Martínez-Cano,[1,5] Iria Sánchez,[1] Diego Mañanes,[1,2] Annalaura Mastrangelo,[1] Joaquín Amores-Iniesta,[1,6] Helena M. Izquierdo,[7,9,*] and David Sancho[1,9,10,*]

[1]Centro Nacional de Investigaciones Cardiovasculares Carlos III, 28029 Madrid, Spain
[2]Escuela de Doctorado, Universidad Autónoma de Madrid, 28049 Madrid, Spain
[3]Facultad de Negocios y Tecnología, Universidad Alfonso X el Sabio (UAX), Villanueva de la Cañada, 28691 Madrid, Spain
[4]Departamento de Inmunología, Oftalmología y ORL, Facultad de Medicina, Universidad Complutense de Madrid, 28040 Madrid, Spain
[5]Inmunotek S.L. Alcalá de Henares, 28805 Madrid, Spain
[6]Grupo de investigación Sanidad de Rumiantes, Departamento de Sanidad Animal, Facultad de Veterinaria, CEIR Campus Mare Nostrum (CMN), Campus de Espinardo, 30100 Murcia, Spain
[7]Institut Curie, PSL University, INSERM U932, Immunity and Cancer, 75005 Paris, France
[8]These authors contributed equally
[9]Senior author
[10]Lead contact
*Correspondence: helena.izquierdo-fernandez@curie.fr (H.M.I.), dsancho@cnic.es (D.S.)
https://doi.org/10.1016/j.celrep.2026.117447

## SUMMARY

Alveolar macrophages (AMs) reside in the oxygen-rich alveoli, where hypoxia-inducible transcription factor (HIF) subunits are targeted for degradation by the Von Hippel-Lindau protein (pVHL). We previously showed that *Vhl*-deficient AMs are immature and functionally impaired. Here, we define isoform-specific roles of HIF-1α and HIF-2α in the regulation of AM maturation and function. Expression of either isoform alone is sufficient to intrinsically, and differentially, impair AM terminal maturation and self-renewal, with complete rescue observed only when both HIF-1α and HIF-2α are deleted in *Vhl*-deficient AMs. HIF-1α drives glycolytic reprogramming in AMs, while HIF-2α disrupts fatty acid oxidation and surfactant clearance. Consequently, HIF-2α stabilization limits the capacity of AMs to resolve surfactant excess in a mouse model of pulmonary alveolar proteinosis, indicating HIF-2α as a potential therapeutic target. Overall, HIF inactivation ensures optimal AM maturation and metabolic adaptation to the high-oxygen alveolar niche, revealing non-redundant functional specificities of each HIF-α isoform.

## INTRODUCTION

Alveolar macrophages (AMs) are lung-resident cells maintained by self-renewal during homeostasis.[1] Through the sensing of granulocyte-macrophage colony-stimulating factor (GM-CSF)[2,3] and transforming growth factor β (TGF-β),[4] fetal liver monocytes differentiate into mature AMs in the lung alveoli during the first week of life. Mature AMs are essential for the regulation of surfactant in the lung, which comprises 90% lipids, and they decrease surface tension. AMs have a remarkable ability for lipid catabolism and cholesterol handling,[5] and these functions are sustained by enzymes and receptors whose expression is regulated by liver-X family of receptors (LXRs), peroxisome proliferator-activated family of receptors (PPARs), CCAAT enhancer-binding proteins (C/EBPs), and sterol regulatory element-binding protein (SREBP) transcription factors.[6] Changes in AM lipid metabolism occur in obstructive pulmonary disease (COPD)[6] and pulmonary alveolar proteinosis (PAP).[7,8] Mechanistically, in mice, deletion of *Pparg*, a master regulator of lipid metabolism induced by GM-CSF, selectively impairs the differentiation of AMs.[3] Depletion of the mitochondrial transcription factor A (TFAM), involved in mitochondrial biogenesis, impairs AM maturation *in vivo*.[5,9] Overall, these studies have identified essential factors for AM maturation and function and demonstrated that alterations in AM metabolism are associated with dysfunction. We have previously shown that Von Hippel-Lindau protein (pVHL) is necessary for AM adaptation to high oxygen levels upon birth and that *Vhl* deletion renders immature and functionally impaired AMs. *Vhl*-deficient AMs present an altered metabolic profile, including enhanced glycolysis and decreased lipid oxidation capacity.[10] However, the role of each hypoxia-inducible transcription factor α (HIF-α) isoform in regulating the functional maturation of AMs has not been investigated.

pVHL is the substrate recognition unit of an E3 ubiquitin ligase complex involved in the ubiquitination and degradation of the alpha isoforms of HIFs in an oxygen-dependent manner.[11–13] HIFs are heterodimeric transcription factors that induce the expression of a set of genes functionally involved in the cellular adaptation to low oxygen tension or hypoxia, including the metabolic switch to glycolysis.[14,15] HIFs are


This is an open access article under the CC BY-NC-ND license (http://creativecommons.org/licenses/by-nc-nd/4.0/).

composed of an oxygen-sensitive α subunit and a constitutive β subunit. Three α subunits have been described (HIF-1α, HIF-2α, and HIF-3α), which heterodimerize with HIF-1β subunit (also named aryl hydrocarbon receptor nuclear translocator 1 [ARNT1]), forming HIF-1, HIF-2, and HIF-3 transcription factors, respectively.[16] When dimerized with the HIF-1β subunit, HIF-1α and HIF-2α regulate the transcription of both shared and distinct target genes. HIF-3α mainly acts as a negative regulator of HIF-1α and HIF-2α by competing for HIF-1β protein available for dimerization, although the HIF-3 dimer also induces the expression of specific genes.[17] Beyond HIF-α regulation, pVHL plays a role in other cellular processes including cytokine signaling, regulation of senescence, formation of extracellular matrix, and mitochondrial function.[18–25] Notably, in our previous work, we found that genes related to the adaptation to hypoxia, including many targets of HIF-1α and HIF-2α, were downregulated within mature AMs after birth.[10] Therefore, we hypothesized that HIF-1α and HIF-2α must be degraded to ensure the correct functional maturation of AMs in steady state.

Here, we investigated the specific function of HIF-1α and HIF-2α in AM phenotypic maturation, self-renewal, and surfactant clearance in the lung. To assess this, we generated four different mouse strains: CD11c-Cre *Vhl*$^{fl/fl}$ (CD11cΔ*Vhl*), CD11c-Cre *Vhl*$^{fl/fl}$*Hif1a*$^{fl/fl}$ (CD11cΔ*Vhl*Δ*Hif1a*), CD11c-Cre *Vhl*$^{fl/fl}$*Hif2a*$^{fl/fl}$ (CD11cΔ*Vhl*Δ*Hif2a*), and CD11c-Cre *Vhl*$^{fl/fl}$*Hif1a*$^{fl/fl}$*Hif2a*$^{fl/fl}$ (CD11cΔ*Vhl*Δ*Hif1a*Δ*Hif2a)*. We demonstrated that the expression of either HIF-1α and HIF-2α alone is sufficient to intrinsically and differentially impair AM terminal maturation and self-renewal, with full rescue observed only in CD11cΔ*Vhl*Δ*Hif1a*Δ*Hif2a* mice. While HIF-1α drives AM metabolic shift toward glycolysis, HIF-2α disrupts lipid oxidation and surfactant clearance, and it is the main isoform responsible for impaired AM maturation. Altogether, this study shows that HIF inactivation ensures the optimal maturation of AMs in the lung, regulating the metabolic adaptation to high oxygen concentration, and highlights different functional specificities of each HIF-α isoform.

## RESULTS

### HIF-1α is the driver of the metabolic switch to glycolysis in *Vhl*-deficient AMs

Our previous work established that pVHL is required for AM phenotypic and functional maturation,[10] but it did not address the specific contribution of HIF-1α and HIF-2α or additional effects of pVHL. To analyze the specific function of HIF-1α and HIF-2α in AMs, we generated four different mouse strains: CD11c-Cre *Vhl*$^{fl/fl}$ (CD11cΔ*Vhl*), CD11c-Cre *Vhl*$^{fl/fl}$*Hif1a*$^{fl/fl}$ (CD11cΔ*Vhl*Δ*Hif1a*), CD11c-Cre *Vhl*$^{fl/fl}$*Hif2a*$^{fl/fl}$ (CD11cΔ*Vhl*Δ*Hif2a*), and CD11c-Cre *Vhl*$^{fl/fl}$*Hif1a*$^{fl/fl}$*Hif2a*$^{fl/fl}$ (CD11cΔ*Vhl*Δ*Hif1a*Δ*Hif2a)*. Analysis of AMs from these mice revealed the expected genotype deficiencies in *Vhl*, *Hif1a*, and *Hif2a* expressions (Figures S1A–S1C), with additional half reduction in *Hif1a* expression levels observed in CD11cΔ*Vhl*Δ*Hif2a* mice (Figure S1B). Consistently, at the protein level, HIF-1α was significantly increased in *Vhl*- and *Vhl*/*Hif2a*-deficient AMs (Figure S1D). HIF-2α protein level was significantly higher in *Vhl*- and *Vhl*/*Hif1a*-deficient AMs (Figure S1E). In contrast, HIF-1α and HIF-2α levels were decreased to wild-type (WT) levels in *Vhl*/*Hif1a*- and *Vhl*/*Hif2a*-deficient AMs, respectively (Figures S1E–S1D), confirming specific and efficient deletion of the corresponding *Hif* gene in each genotype.

To investigate the contribution of HIF-1α and HIF-2α to the immature-like phenotype found in *Vhl*-deficient AMs,[10,26] we performed RNA sequencing (RNA-seq) of the AMs isolated from all the mouse strains compared with their respective Cre-negative littermate control mice. Analysis of differentially expressed genes (DEGs) showed that a total of 1,246 genes expressed, with at least a 2-fold difference (adj. $p < 0.01$). In CD11cΔ*Vhl*Δ*Hif1a*Δ*Hif2a* AMs, only *Vhl* and *Plcb4* were differentially expressed (Figures 1A–1D), showing that the transcriptional changes seen in *Vhl*-deficient AM rely exclusively on the downstream transcription factors HIF-1α and HIF-2α, rather than on HIF-independent pVHL functions. Principal-component analysis (PCA) showed that samples from CD11cΔ*Vhl*Δ*Hif1a*Δ*Hif2a* scored close to those of controls and distant from those of CD11cΔ*Vhl*, CD11cΔ*Vhl*Δ*Hif1a*, and CD11cΔ*Vhl*Δ*Hif2a* in principle component 1 (PC1; Figure 1E), supporting the total HIF dependency of pVHL functions.

Different genes were deregulated in AMs depending on the genotype (Figures S2A–S2C). Pre-ranked gene set enrichment analysis of genes with the greatest contribution to PC1 unveiled pathways related to cell division and metabolism, suggesting that both HIF-1α and HIF-2α are involved in their regulation (Figure 1F). To further interrogate the specific contribution of each HIF isoform, we performed an overrepresentation analysis (ORA) along with the Kyoto Encyclopedia of Genes and Genomes (KEGG) pathway database analysis of DEGs from each genotype. "PPAR signaling," "HIF1A signaling," and "glycolysis/gluconeogenesis" were identified as upregulated pathways that were only partially restored by deficiency of either HIF-1α or HIF-2α, indicating that both transcription factors regulate these programs (Figure S2D). We also found pathways similarly controlled by both HIF isoforms, such as "AMPK" or "PI3K-Akt signaling pathways" (Figure S2D), suggesting that either HIF isoform is sufficient to activate these pathways (Figure S2D). Finally, most downregulated pathways were shared between *Vhl*- and *Vhl*/*Hif2a*-deficient AMs, pointing to HIF-1α as their main regulator (Figure S2D).

HIF-1α and HIF-2α induce the transcription of common target genes involved in response to hypoxia. However, stable activation of HIF isoforms with prolonged hypoxia can result in the predominance of HIF-2α activity rather than HIF-1α.[27] To characterize the contribution of each HIF isoform to these specific pathways in *Vhl*-deficient AMs, we compared the core gene expression signature associated with the "response to the hypoxia" KEGG pathway. The upregulated genes found in *Vhl*-deficient AMs were restored by further deletion of *Hif1a* but not *Hif2a* (Figure S2E). The same was true for DEGs associated with the KEGG pathways "oxidative phosphorylation" (OxPhos) and "glycolysis" (Figures S2F and S2G), suggesting that HIF-1α is the main regulator of these gene sets over HIF-2α in AMs. We also found that deleting *Hif2a* in *Vhl*-deficient AMs further amplified the transcriptional changes associated with the response to hypoxia, observed in *Vhl* deletion alone (Figures S2F and S2G). This suggests that *Hif2a* plays a negative regulatory role in these pathways and is consistent with the significant increase in HIF-1α protein level observed in *Vhl*/*Hif2a*-deficient AMs compared with WT controls (Figure S1D).

CellPress
OPEN ACCESS

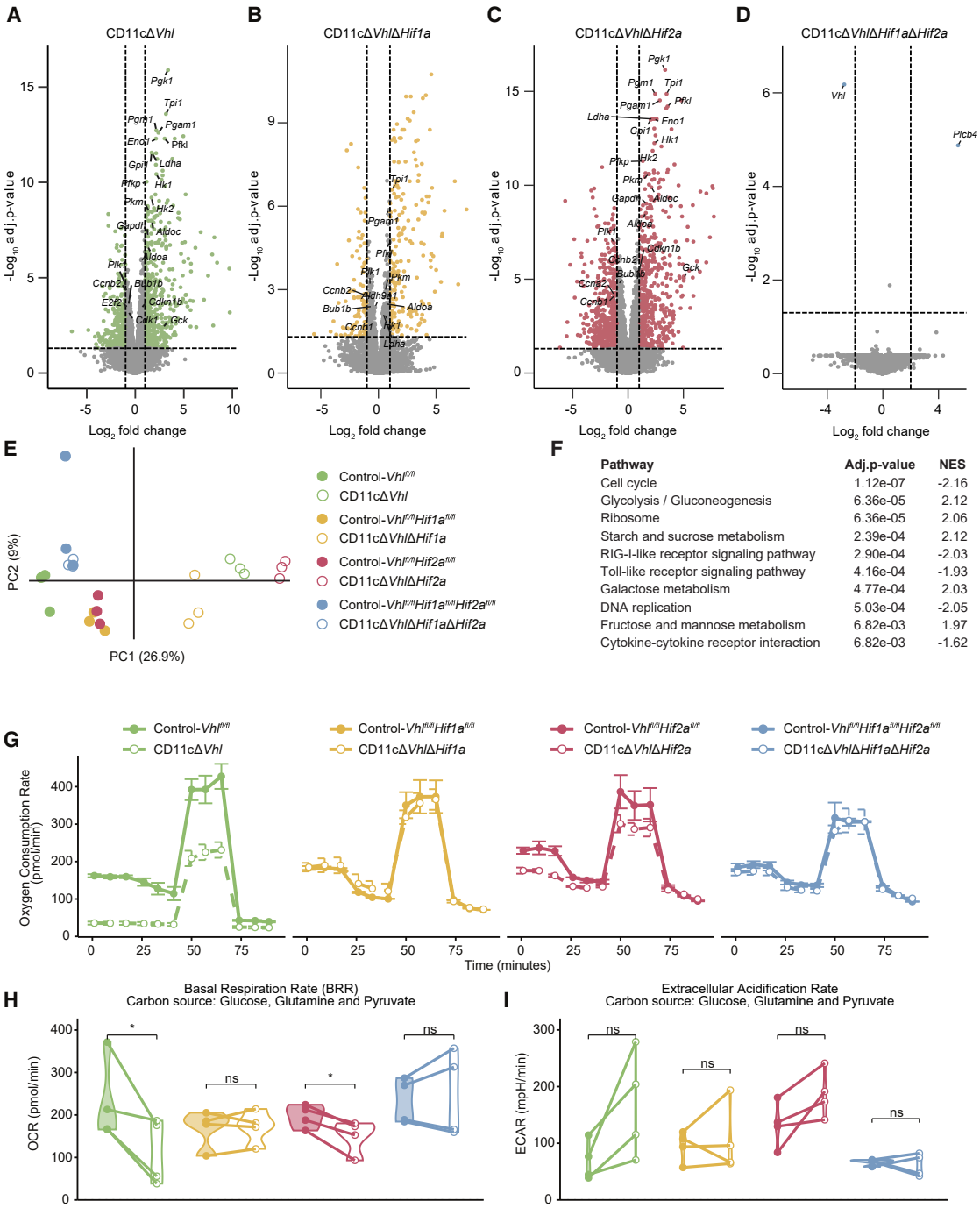



**Figure 1. HIF-1α drives glycolysis in *Vhl*-deficient AMs**

(A–D) Volcano plots of differentially expressed genes ranked, showing adjusted *p* value ($log_{10}$ adj. *p* value) and $log_2$ fold change between AMs from CD11cΔ*Vhl* (A), CD11cΔ*VhlΔHif1a* (B), CD11cΔ*VhlΔHif2a* (C), and CD11cΔ*VhlΔHif1aΔHif2a* (D) mice compared to their littermate control; differentially expressed genes (adjusted *p* value < 0.05 and abs($log_2$FC) > 1) are depicted in the color code associated with each genotype.

(E) Principal-component analysis (PCA) of the transcriptomic profiles of AMs from CD11cΔ*Vhl*, CD11cΔ*VhlΔHif1a*, CD11cΔ*VhlΔHif2a*, CD11cΔ*VhlΔHif1aΔHif2a* mice, and their littermate controls. Each dot represents a pool of 2–3 mice.

(F) Pre-ranked enrichment analysis of the genes defining PC1 using KEGG pathways. NES, normalized enrichment score; *p* value was adjusted with Benjamin-Hochberg correction.

(G) Oxygen consumption rate (OCR) by BAL AMs cultured in media containing glucose, glutamine, and pyruvate. Data are shown as the mean ± SD.

(H and I) Basal respiratory rate (BRR) (H) and extracellular acidification rate (ECAR) (I) of BAL AMs. Each dot represents a pool of *n* = 6–7 mice per genotype. Paired Student's *t* test; *, *p* < 0.05; ns, not significant.

See also Figures S1–S3.

To further define which pathways downregulated during postnatal AM maturation are controlled by HIFs, we analyzed the transcriptional datasets, focusing on genes reduced in mature adult AMs ("adult") relative to immature AM precursors at postnatal day 2 (P2) from the Schneider et al.'s dataset.[3] Because HIFs primarily act as gene expression activators,[28] we next examined genes upregulated in *Vhl*-, *Vhl*/*Hif1a*-, and *Vhl*/*Hif2a*-deficient AMs relative to those in their respective WT counterparts and determined their overlap with the adult vs. P2 gene dataset (Figure S3A). ORA of genes at intersections identified "glycolysis/gluconeogenesis" as the top pathway downregulated during AM maturation and enriched in immature-like *Vhl*-deficient AMs (Figure S3B). Notably, this pathway was not enriched in *Vhl*/*Hif1a*-deficient AMs, supporting a central role for HIF-1α in maintaining immature metabolic programs (Figure S3B). In contrast, the glucagon signaling remained enriched in *Vhl*-deficient AMs and appeared to be mainly regulated by HIF-2α (Figure S3B).

Real-time metabolic profiles of AMs in the presence of glucose, pyruvate, and glutamine by Seahorse showed that CD11cΔ*Vhl* and CD11cΔ*Vhl*Δ*Hif2a* AMs exhibited a significantly decreased basal respiratory rate (BRR) while maintaining the extracellular acidification rate (ECAR) compared with those of controls, reflecting a decreased use of glucose for the tricarboxylic acid (TCA) and mitochondrial OxPhos toward an enhanced aerobic glycolysis and lactate production. In contrast, CD11cΔ*Vhl*Δ*Hif1a* and CD11cΔ*Vhl*Δ*Hif1a*Δ*Hif2a* AMs showed the BRR and ECAR similar to those of WT (Figures 1G and 1H). Together, these findings support that HIF inactivation is required for proper AM functional postnatal maturation and that pVHL loss disrupts this process primarily through HIF-1α-dependent transcriptional metabolic reprogramming including hypoxia-, glycolysis- and OxPhos-related genes, with HIF-2α contributing to targeted metabolic alterations. Consistently, HIF-1α emerges as the key driver of the metabolic switch toward glycolysis in *Vhl*-deficient AMs.

## HIF-1α and HIF-2α differentially regulate AM identity genes in CD11cΔ*Vhl* mice

We have previously shown that *Vhl*-deficient AMs showed an altered expression of surface markers,[10] akin to immature cells.[2] We then asked which HIF isoform dampens mature AM identity in the absence of pVHL. We compared the expression of classical surface markers that are associated with AM maturation status. While the expression pattern of maturation markers such as CD11c, Siglec-F, CD11b, or MHC class II (I-A/I-E) was restored to control WT expression in CD11cΔ*Vhl*Δ*Hif1a*Δ*Hif2a*, most of the changes in marker expression found in CD11cΔ*Vhl* mice remained unchanged or were partially restored upon further depletion of HIF-1α. In contrast, most of these changes were largely reversed upon HIF-2α depletion (Figures 2A–2E). We then compared the unique AM gene expression signature that was identified by the ImmGen consortium.[29] Notably, we found three distinct sets of genes: (1) genes regulated by HIF-2α, with functions in lipid metabolism (*Lsr*, *Vstm2a*, and *Cidec*); (2) genes regulated by HIF-1α, involved in a plethora of functions including regulation of cytoskeleton (*Clmn*, *Sema3e*, *Krt19*, *Matn2*, and *Itgax*), circadian clock genes (*Ear1* and *Rara*), and cell metabolism (*Lepr, Naaa, Acaa1b, Aldoc*, and *Fabp1*); and (3) a third set of genes regulated by both HIF-1α and HIF-2α (Figure 2F). Overall, our data indicate that although deleting HIF-2α in *Vhl*-deficient AMs substantially restores most control WT surface marker expression, both HIF isoforms, independently or in combination, contribute to shaping the underlying transcriptional identity of mature AMs (Figure 2F).

## AM self-renewal capacity is impaired by both HIF-1α and HIF-2α in CD11cΔ*Vhl* mice

AMs are lung-resident cells maintained locally by self-renewal at the steady state.[30] Enhanced glycolysis correlates with reduced AM self-renewal capacity,[5,10,26] but its association with specific HIF isoforms remains unclear. Thus, we next investigated which HIF isoform was regulating AM proliferation in *Vhl*-deficient AMs. The percentage of Ki67$^+$ AMs was significantly and similarly reduced in CD11cΔ*Vhl*Δ*Hif1a* and CD11cΔ*Vhl*Δ*Hif2a* AMs, indicating that both isoforms contribute to the defective proliferation in the absence of pVHL (Figure 3A). In contrast, it was completely restored to control WT expression in CD11cΔ*Vhl*Δ*Hif1a*Δ*Hif2a* AMs (Figure 3A). In agreement, the differential expression of genes related to cell cycle-associated genes in CD11cΔ*Vhl* AMs showed a similar pattern when either *Hif1a* or *Hif2a* was individually deleted (Figure S4A). Furthermore, BrdU uptake in *ex vivo* AM cultures with GM-CSF showed recovery of their full proliferative capacity only in the *Vhl*/*Hif1a*/*Hif2a* triple knockouts (Figure 3B). Overall, these results demonstrate that both HIF-1α and HIF-2α impair AM stemness independently of glycolysis and other environmental (extrinsic) factors.

AMs can differentiate from circulating monocytes coming from bone marrow precursors.[30] We then asked whether the previously observed compromised AM proliferative capacity constitutes a selective disadvantage at reconstituting an empty niche in the context of competence with WT AMs. To address this, we generated bone marrow mixed chimeras: lethally irradiated CD45.1$^+$ recipients were transferred intravenously with bone marrow cells from CD45.1$^+$CD45.2$^+$ WT control and CD45.2$^+$ CD11cΔ*Vhl*, CD11cΔ*Vhl*Δ*Hif1a*, CD11cΔ*Vhl*Δ*Hif2a*, CD11cΔ*Vhl*Δ*Hif1a*Δ*Hif2a*, or their control Flox littermates in a 1:1 ratio (Figure 3C). After 1.5 months, similar numbers of total AMs were found in all the chimeric mice, ruling out the differences in niche accessibility (Figure S4B). Frequencies of blood neutrophils and monocytes from CD45.1$^+$CD45.2$^+$ and CD45.2$^+$ mice were also similar, indicating an equally efficient bone marrow reconstitution (Figures S4C and S4D). In the bronchoalveolar lavage (BAL), CD45.2$^+$ CD11cΔ*Vhl* and CD11cΔ*Vhl*Δ*Hif2a* monocyte-derived AMs were significantly less abundant than CD45.1$^+$CD45.2$^+$ control WT cells (Figure 3D), correlating with a decreased frequency of Ki67$^+$ AMs (Figures 3E and 3F). Unexpectedly, CD11cΔ*Vhl*Δ*Hif1a* monocyte-derived AMs also showed a significantly reduced percentage of Ki67$^+$ cells but reconstituted the alveolar niche as efficiently as control WT AMs, suggesting a survival advantage (Figures 3D–3F). These results indicate that while both HIF isoforms regulate AM self-renewal capacity, HIF-1α appears to be the main driver of the impaired alveolar niche reconstitution in the absence of pVHL.

In the bone marrow-graft model, CD11cΔ*Vhl*, CD11cΔ*Vhl*Δ*Hif1a*, and CD11cΔ*Vhl*Δ*Hif2a* monocyte-derived AMs expressed similar

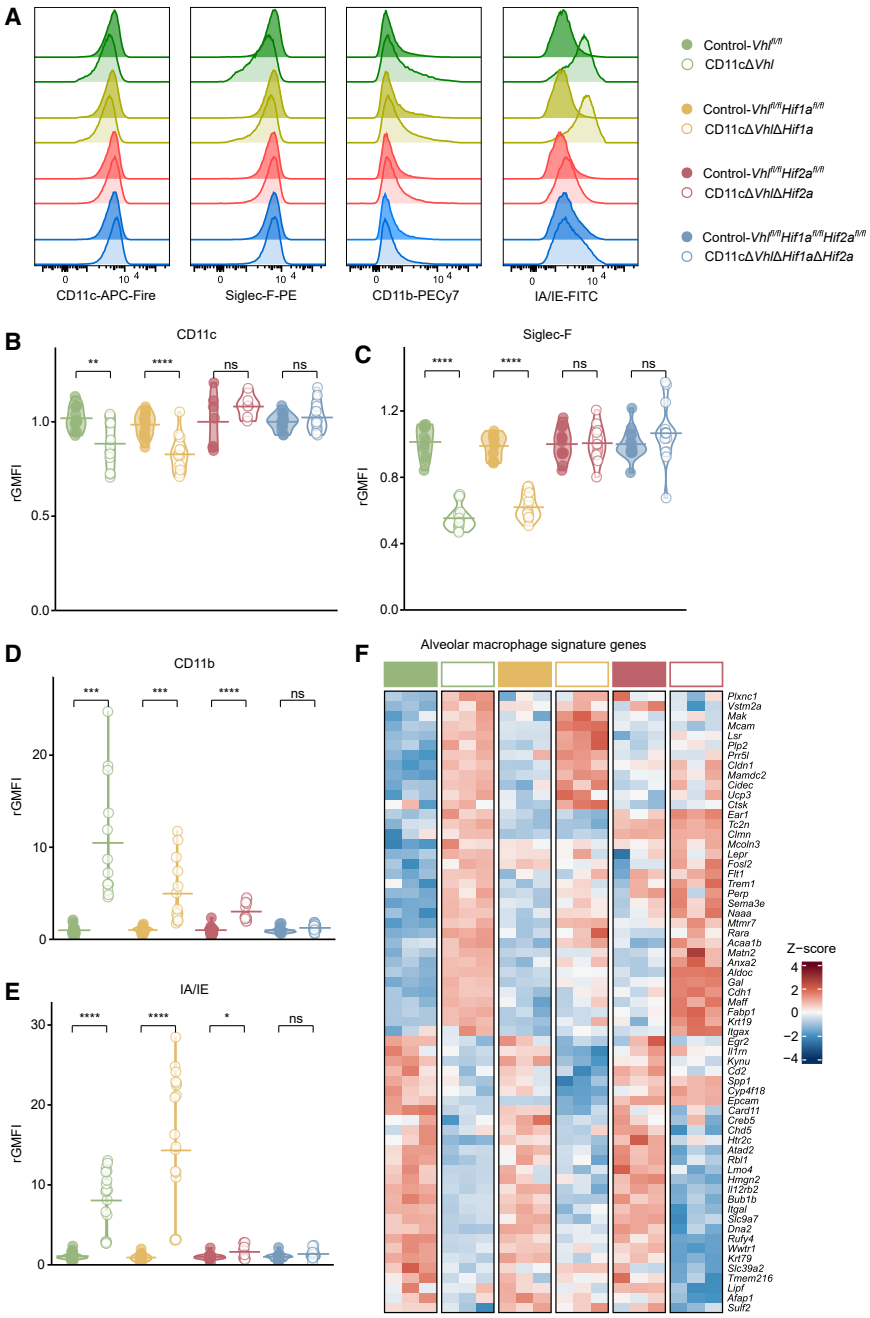



**Figure 2. Mature AM transcriptional signature relies on HIF inactivation**

(A) Representative flow cytometry histograms for CD11c, Siglec-F, CD11b, and IA/IE expression by BAL AMs from the indicated genotypes.

(B–E) Quantification of the geometric mean of fluoresce intensity (GMFI) relative to the mean value of control samples (rGMFI) of CD11c (B), Siglec-F (C), CD11b (D), and IA/IE (E). Pool of 2–3 experiments; $n = 4$–6 mice per experiment, bar indicates mean of the GMFI values. Student's $t$ test. ****, $p < 0.0001$; ***, $p < 0.001$; **, $p < 0.01$; *, $p < 0.05$; ns, not significant.

(F) Gene expression heatmap of the lung AM-specific signature gene set described by Gautier et al.[29]

levels of CD11c (Figure 3G). Monocyte-derived AMs from CD11cΔ*Vhl*Δ*Hif1a*Δ*Hif2a* mice fully recapitulated the expression of all surface markers observed in CD45.1$^+$CD45.2$^+$ WT controls. In contrast, both CD11cΔ*Vhl*Δ*Hif1a* and CD11cΔ*Vhl*Δ*Hif2a* monocyte-derived AMs only partially restored CD11b and Siglec-F expression (Figures 3H–3J). Notably, CD11cΔ*Vhl*Δ*Hif2a* monocyte-derived AMs completely restored MHC class II (I-A/I-E) expression, akin to the phenotype of *Vhl*/*Hif2a*-deficient AMs (Figure 2E). AMs from WT littermates showed frequencies of Ki67$^+$ and levels of surface markers similar to CD45.1$^+$CD45.2$^+$ WT

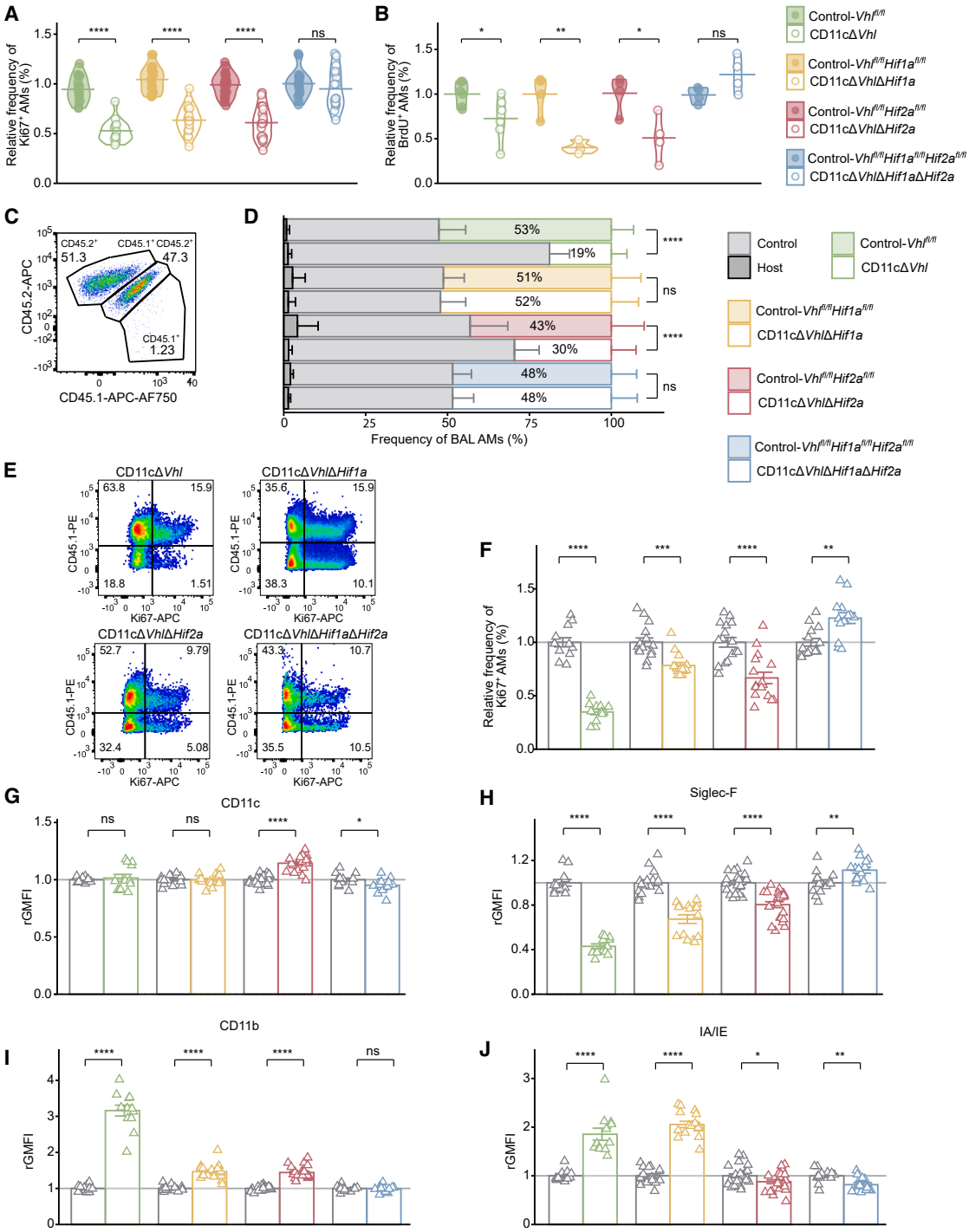



**Figure 3. Both HIF isoforms interfere with AM self-renewal**

(A) Quantification of the frequency of Ki67$^+$ BAL AMs relativized to the mean value for WT. Pool of 3 experiments; $n = 5–8$ mice per experiment, bar indicates mean. Student's $t$ test, ****, $p < 0.0001$; ns, not significant.

(B) Quantification of the frequency of BrdU$^+$ BAL AMs after 3 days in culture with rGM-CSF. Pool of 2 experiments, with each dot representing a pool of $n = 15–18$ mice per experiment, bar indicates mean. Student's $t$ test, **, $p < 0.01$; *, $p < 0.05$; ns, not significant.

(C) Representative dot plot showing the percentage of host CD45.1$^+$, control transplanted CD45.1$^+$CD45.2$^+$, and experimental transplanted CD45.2$^+$ cells, gated within Siglec-F$^+$ CD11c$^+$ BAL AMs.

(D) Quantification of the percentage of each AM subpopulation. Bar indicates the mean ± SEM. Student's $t$ test, Student's $t$ test, ****, $p < 0.0001$; ns, not significant.

*(legend continued on next page)*

controls (Figures S4E–S4I). These results confirmed that the HIF-dependent defect in the maturation and proliferation of *Vhl*-deficient AMs is cell intrinsic.

### HIF-2α selectively compromises surfactant clearance capacity by *Vhl*-deficient AMs

In lung alveoli, AMs play a major role, degrading the surfactant produced by lung type II epithelial cells. Genetic defects in GM-CSF signaling prevent AM maturation and lead to the development of spontaneous PAP, characterized by the accumulation of the surfactant.[31] HIF-1α-mediated switch to glycolysis has been linked to the accumulation of lipids and the development of foam cells.[32–34] We previously reported that CD11cΔ*Vhl* AMs have a decreased capacity to oxidize lipids *ex vivo* and, consequently, when adoptively transferred to *Cfsr2*$^{-/-}$ mice, which lack AMs and develop PAP spontaneously, they are not able to reduce the surfactant content in the alveoli.[10] To interrogate into the regulation of lipid metabolism by HIF-1α or HIF-2α *in vivo*, we intratracheally transferred AMs from CD11cΔ*Vhl*Δ*Hif1a*, CD11cΔ*Vhl*Δ*Hif2a*, CD11cΔ*Vhl*Δ*Hif1a*Δ*Hif2a*, or their control counterparts into *Cfsr2*$^{-/-}$ mice. Only adoptively transferred CD11cΔ*Vhl*Δ*Hif2a* AMs and CD11cΔ*Vhl*Δ*Hif1a*Δ*Hif2a* AMs were able to decrease the total protein and specific surfactant protein D (SP-D) in BAL to levels similar to those of WT (Figures 4A and 4B), indicating that HIF-2α stabilization impairs surfactant clearance by lung AMs. Similar numbers of AMs were recovered from BAL for all genotypes, indicating the same efficiency at replenishing the lung alveoli (Figure S5A).

AMs rely on fatty acid oxidation and cholesterol efflux to metabolize lipids and avoid their accumulation, respectively.[5] To assess the regulation of lipid oxidation by HIF isoforms in a controlled *in vitro* setting, we conducted real-time metabolic profile with palmitoyl-CoA as the only carbon source. The BRR was significantly reduced in CD11cΔ*Vhl* and CD11cΔ*Vhl*Δ*Hif1a* AMs compared with WT, but it was completely restored in CD11cΔ*Vhl*Δ*Hif2a* and CD11cΔ*Vhl*Δ*Hif1a*Δ*Hif2a* AMs (Figure 4C).

We then compared the expression of fatty acid and cholesterol metabolism-related genes among genotypes. In agreement with our *in vivo* and *in vitro* results, we found the expression of multiple DEGs associated with fatty acid oxidation in *Vhl*-deficient AMs in CD11cΔ*Vhl*Δ*Hif1a*, but WT expression profile was restored in CD11cΔ*Vhl*Δ*Hif2a* AMs (Figure 4D). Globally, these results highlight HIF-2α as a major regulator of fatty acid oxidation in lung AMs.

## DISCUSSION

AMs derive from embryonic progenitors that colonize the lung alveoli and undergo maturation after birth. Maturation onset coincides with the exposure of the alveoli to high oxygen concentrations upon the first breath. We previously showed that the genes related to the adaptation to hypoxia, including HIF-target genes, are downregulated during AM maturation.[10] The role of HIF-1α has been well studied in monocyte-derived macrophages, where it plays a major role in macrophage infiltration and proinflammatory responses.[35–39] Influenza infection is associated with lung edema and cellular infiltrations, which can result in hypoxia.[40,41] HIF-1α stabilization has been reported in lung AMs upon influenza infection, leading to glycolysis induction.[42] However, the role of HIF isoforms in AM metabolic adaptation to their niche in homeostasis is largely unknown. In the present study, we have uncovered that HIF-1α and HIF-2α differentially impair specific AM functions. Thus, the inactivation of HIF function is essential for lung AM functional maturation. Our transcriptional analysis indicates that glycolysis is downregulated in mature adult AMs compared with postnatal day 2 precursors but upregulated in *Vhl*-deficient AMs relative to controls. We demonstrated that HIF-1α is the exclusive driver of this glycolytic switch in *Vhl*-deficient AMs. Overall, these results indicate that HIF-1α inactivation is required for proper AM functional maturation, in part, through reprogramming of the metabolic trajectory of the developing AM precursors. Notably, both HIF-1α and HIF-2α play a role in the phenotypic maturation and transcriptional identity of AMs, corroborated by the cell-intrinsic nature of the altered surface marker expression found in monocyte-derived AM deficient in *Vhl, Vhl/Hif1a*, and *Vhl/Hif2a*. HIF-1α stabilization leads to the expression of the antimicrobial enzyme iNOS[43] and is protective against lung fibrosis.[26] This suggests that HIF activation in response to certain exogenous stimuli can be beneficial, whereas under sterile conditions, it must be tightly regulated.

Increased glycolysis has been linked to the decreased self-renewal potential in AMs.[5,44] Ki67 expression and BrdU uptake assays indicated that both HIF-1α and HIF-2α similarly impair AM proliferation in the absence of pVHL. Despite significant defect in the proliferation of *Vhl*-deficient AMs, total numbers in the lung alveoli were similar to those of WT, suggesting that they can fully replenish the alveolar niche in the absence of competition from incoming blood monocytes. Mixed bone marrow chimeras confirmed that *Vhl*-deficient AM immature phenotype and defective proliferation are cell intrinsic and that *Vhl*- and *Vhl/Hif2a*-deficient AMs are significantly outcompeted by control WT AMs. In contrast, *Vhl/Hif1a*-deficient AMs were similarly able to repopulate the alveoli despite decreased Ki67 expression. This effect may be linked to the pro-survival role of HIF-2α,[45] although further investigation is required. The chimera model enables circulating monocytes to enter the alveolar niche and differentiate, resembling the postnatal maturation of

(E) Representative dot plots showing Ki67 expression by CD45.2$^+$ Siglec-F$^+$CD11c$^+$ gated BAL AMs 45 days after BM transfer, in which CD45.1$^+$ and CD45.1$^-$ correspond to control and experimentally transplanted, respectively.
(F) Quantification of the frequency of Ki67$^+$ AMs of each genotype relativized to the mean value for control CD45.1$^+$ AMs. Bar indicates the mean ± SEM. Student's *t* test, ****, $p < 0.0001$; ***, $p < 0.001$; **, $p < 0.01$.
(G–J) Quantification of the GMFI relative to the mean value of control CD45.1$^+$ AM samples (rGMFI) of CD11c (G), Siglec-F (H), CD11b (I), and IA/IE (J). Bar indicates the mean ± SEM. Student's *t* test, ****, $p < 0.0001$; ***, $p < 0.001$; **, $p < 0.01$; *, $p < 0.05$; ns, not significant.
(D)–(J) show pool of experiments, with $n = 6–8$ chimeras per experiment.
See also Figure S4.

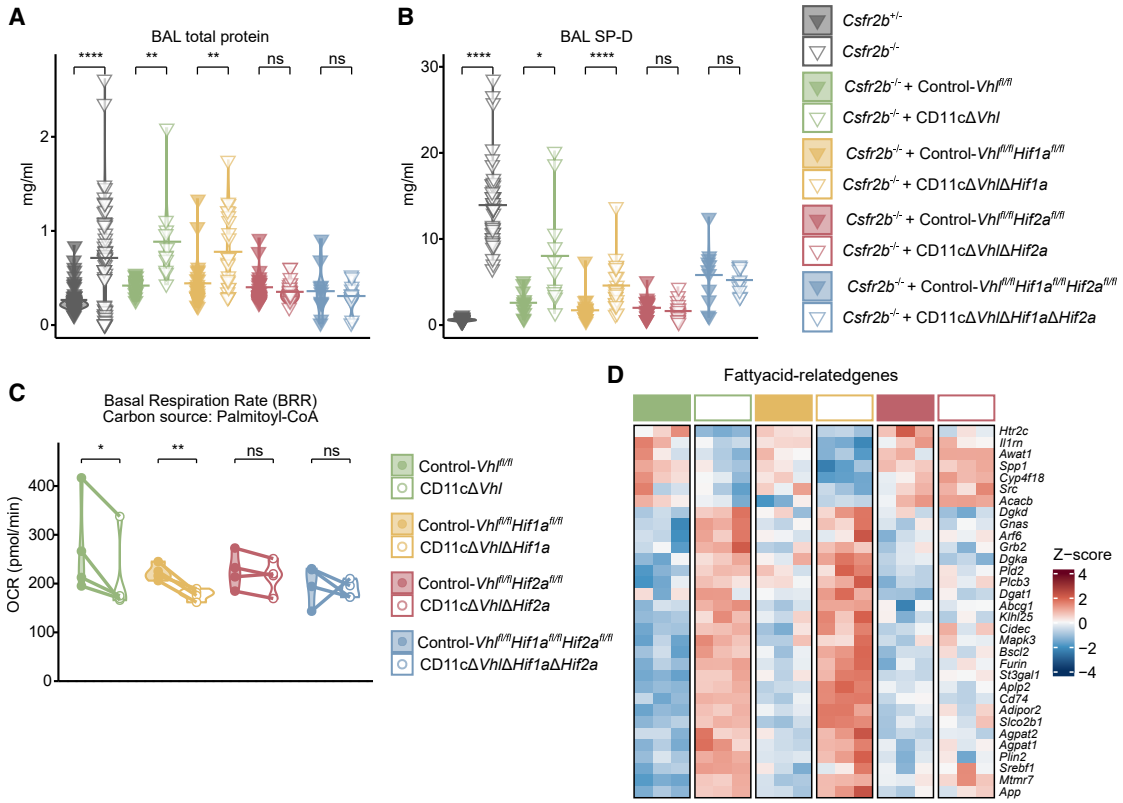



**Figure 4. HIF-2α impairs fatty acid oxidation and surfactant clearance by AMs**

(A and B) Quantification of total protein (A) and surfactant protein D (SP-D) (B) in BAL fluid from Csfr2b$^{-/-}$ mice transplanted with BAL AMs from the indicated genotypes. Control mice (Csfr2b$^{-/-}$ and Csfr2b$^{+/-}$) were pooled from each independent experiment. Pool of 3 experiments, with $n$ = 3–10 mice per experiment, bars indicate mean. Student's $t$ test; ****, $p < 0.0001$; **, $p < 0.01$; *, $p < 0.05$; ns, not significant.

(C) Quantification of the basal respiratory rate (BRR) of BAL AMs in media containing palmitoyl-CoA and L-carnitine. Pool of 4 experiments, with each dot representing a pool of $n$ = 6–7 mice. Student's $t$ test; **, $p < 0.01$; *, $p < 0.05$; ns, not significant.

(D) Heatmap showing differential expression of genes related to lipid metabolic process GO pathway (GO:0019216) in the indicated genotypes.

See also Figure S5.

embryonically seeded precursors into fully differentiated AMs.[30] Using this approach, we confirmed that HIF signaling impairs both the phenotypical and functional maturation of AMs, independent of their developmental origin.

Notably, we found that compared with *Vhl*/*Hif1a*-deficient AMs, *Vhl*/*Hif2a*-deficient AMs had impaired oxidative capacity in the presence of glucose and glutamine. In contrast, *Vhl*/*Hif1a*-deficient AMs showed a decreased oxygen consumption when palmitoyl-CoA was used as the substrate, a phenomenon not observed in *Vhl*/*Hif2a*-deficient AMs. The specific roles of HIF-1α and HIF-2α in the regulation of lipid metabolism pathways are still controversial. HIF-2α plays a dominant role in hepatic steatosis through fatty acid oxidation impairment upon depletion of pVHL.[46] In contrast, HIF-1α was reported to enhance hepatic lipid accumulation in a model of alcoholic fatty liver disease.[33] Another study showed that deletion of both HIF isoforms is sufficient to ameliorate lipid accumulation induced by hypoxia in the HepG2 cell line.[47] Discrepancy among these results may be due to the different triggers used to activate HIF (pVHL depletion, alcohol, and hypoxia, respectively), which likely involves a different dynamic of HIF isoform activation.[27] In the case of monocyte-derived macrophages (MDMs), under hypoxia, they accumulate lipids and become foam cells, which correlates with the activation of HIF-1α.[32] HIF-1α was reported to prevent cholesterol efflux, contributing to lipid accumulation in a macrophage cell line.[34] However, MDMs strongly rely on glycolysis compared with lung AMs at a basal level,[48] suggesting that the metabolic regulation of MDMs cannot be extrapolated to tissue-resident macrophages. In agreement, a recent study has shown that lung AMs are enriched in a fatty acid oxidation module, including enzymes involved in lysosomal lipolysis, mitochondrial fatty acid import, and oxidation,[49] Our results unveiled HIF-2α as the key regulator of lipid oxidation in lung AMs. *Vhl*/*Hif2a*-deficient AMs could completely restore homeostatic levels of the surfactant upon being transplanted into a mouse model of PAP and restore basal OCR levels when palmitoyl-CoA was used as the carbon substrate *in vitro*. Overall, this work demonstrates the specific roles of HIF-1α and HIF-2α in fine-tuning lung AM gene expression and functions. Our results highlight the importance of developing therapies targeting each HIF isoform and unveil HIF-2α as a potential target to improve surfactant removal in secondary PAP diseases.

### Limitations of the study

Our study delineates the relative contributions of HIF-1α and HIF-2α to the regulation of AM functional maturation after birth. Several limitations should be acknowledged. First, our conclusions rely primarily on genetic models in which HIF signaling is constantly stabilized through *Vhl* deletion. This approach results in sustained, high HIF activity that may not accurately reflect physiological prenatal HIF signaling. Direct quantification of HIF-1α and HIF-2α protein abundances in WT mice during the prenatal stage, coupled with comparative analysis in WT and *Vhl*-deficient AMs, would help establish the physiological relevance of our findings. Second, although we identified consistent changes in maturation programs, self-renewal capacity, and fatty acid oxidation upon HIF-1α and HIF-2α stabilization, we did not define the precise underlying molecular mechanisms. Some effects are likely mediated by direct transcriptional activation of HIF target genes, whereas others may arise from indirect regulatory networks or secondary metabolic adaptations. Consequently, additional mechanistic studies, such as chromatin immunoprecipitation sequencing (ChIP-seq) (or CUT&RUN or CUT&Tag), to map HIF-1α and HIF-2α occupancy, combined with targeted perturbation or rescue of candidate downstream effectors, will be required to determine the causal links between HIF transcriptional activity and the observed phenotypes. Finally, while we defined isoform-specific roles for HIF-1α and HIF-2α in AMs under homeostatic conditions, their specific contributions during environmental sensing, such as hypoxic stress, inflammation, or tissue injury, remain unexplored and warrant future investigation.

## RESOURCE AVAILABILITY

### Lead contact

Requests for further information and resources should be directed to and will be fulfilled by the lead contact, David Sancho (dsancho@cnic.es).

### Materials availability

*Itgax*$^{Cre}$*Vhl*$^{fl/fl}$, *Itgax*$^{Cre}$*Vhl*$^{fl/fl}$*Hif1a*$^{fl/fl}$, *Itgax*$^{Cre}$*Vhl*$^{fl/fl}$*Hif2a*$^{fl/fl}$, and *Itgax*$^{Cre}$*Vhl*$^{fl/fl}$ *Hif1a*$^{fl/fl}$*Hif2a*$^{fl/fl}$ mice are available upon request.

### Data and code availability

- Bulk RNA-seq data of CD11cΔ*Vhl*Δ*Hif1a*, CD11cΔ*Vhl*Δ*Hif2a*, and CD11cΔ*Vhl*Δ*Hif1a*Δ*Hif2a* AMs and their respective controls have been deposited at GEO, with accession number GEO: GSE325293, and will be publicly available as of the date of publication.
- Bulk RNA-seq data of control vs. CD11cΔ*Vhl* AMs were deposited at GEO (GEO: GSE108975) in a previous study by our group.[10]
- Microarray data (CEL files) of P2 vs. adult AMs[3] are publicly available at GEO under accession number GEO: GSE60249.
- Original code and data have been deposited at Zenodo and are available as of date of publication (Zenodo: https://doi.org/10.5281/zenodo.18965962 and Zenodo: https://doi.org/10.5281/zenodo.19183042).
- Any additional information required to reanalyze the data reported in this paper is available upon request to the lead contact.

## ACKNOWLEDGMENTS

We thank members of the D.S. laboratory at CNIC, past and present, for feedback and scientific discussions on this project and manuscript. We also thank all CNIC facilities and assistants for their support. Work in the DS laboratory was supported by the CNIC; Ministerio de Ciencia, Innovación y Universidades (MICIU) PID2022-137712OB-I00, PDC2025-165319-I00, CPP2022-009762, and CPP2024-011365 MICIU/AEI/10.13039/501100011033 Agencia Estatal de Investigación, Unión Europea NextGenerationEU/PRTR; Comunidad de Madrid (P2022/BMD-7333 INMUNOVAR-CM); Scientific Foundation of the Spanish Association Against Cancer (AECC-PRYGN246642SANC); Worldwide Cancer Research WWCR-25-0080; Fundación CRIS contra el cáncer (excellence2025_03); and "la Caixa" Foundation (LCF/PR/HR23/52430012 and LCF/PR/HR22/52420019). E.P. was funded by Contratos Predoctorales para la Formación de Doctores 2017 (BES-2017-079717), I.A.-B. was supported by a Beca de Formación del Profesorado Universitario fellowship (FPU18/05752) and by PID2021-125415OB-I00 from the Spanish Ministry of Science. H.M.I. was funded by fellowships from the French Agency for Research on AIDS and Viral Hepatitis, ANRS (ECTZ171453), the Spanish Foundation Séneca (20941/PD/18), and the Institut Curie (fellowship for foreign postdocs). The CNIC is supported by the Instituto de Salud Carlos III (ISCIII), the MICIU and the Pro CNIC Foundation, and is a Severo Ochoa Center of Excellence (CEX2020-001041-S funded by MICIU/AEI/10.13039/501100011033).

## AUTHOR CONTRIBUTIONS

Conceptualization, H.M.I. and D.S.; methodology, E.P., I.A.-B., and D.S.; investigation, E.P., I.A-B., R.C.-G., S.M.-C., I.S., and J.A.-I.; formal analysis, E.P., I.A.-B., D.M., A.M., H.M.I., and D.S.; resources, R.C.-G., S.M.-C., I.S., and J.A.-I.; writing – original draft, E.P., I.A.-B., H.M.I., and D.S.; writing – review & editing, all authors; supervision, H.M.I. and D.S.; project administration and funding acquisition, D.S.

## DECLARATION OF INTERESTS

The authors declare no competing interests.

## DECLARATION OF GENERATIVE AI AND AI-ASSISTED TECHNOLOGIES IN THE WRITING PROCESS

During the preparation of this work, the authors used M365 Copilot to refine language and improve clarity in the text. After using this tool, the authors reviewed and edited the content as needed and take full responsibility for the content of the publication.

## STAR★METHODS

Detailed methods are provided in the online version of this paper and include the following:

- KEY RESOURCES TABLE
- EXPERIMENTAL MODEL AND STUDY PARTICIPANT DETAILS
  - Animal models
- METHOD DETAILS
  - AM isolation
  - AM *in vitro* culture
  - Flow cytometry
  - Real-time oxygen consumption rate and glycolytic flux
  - RNA sequencing and analysis
  - Analysis of public GSE60249 microarray data and over-representation analysis
  - Bone marrow transfer mixed chimeras
  - Pulmonary macrophage transplantation
- QUANTIFICATION AND STATISTICAL ANALYSIS

## SUPPLEMENTAL INFORMATION

Supplemental information can be found online at https://doi.org/10.1016/j.celrep.2026.117447.

Received: July 20, 2025
Revised: March 27, 2026
Accepted: May 6, 2026
Published: May 28, 2026

## REFERENCES


1. Hashimoto, D., Chow, A., Noizat, C., Teo, P., Beasley, M.B., Leboeuf, M., Becker, C.D., See, P., Price, J., Lucas, D., et al. (2013). Tissue-Resident Macrophages Self-Maintain Locally throughout Adult Life with Minimal Contribution from Circulating Monocytes. Immunity *38*, 792–804. https://doi.org/10.1016/j.immuni.2013.04.004.
2. Guilliams, M., De Kleer, I., Henri, S., Post, S., Vanhoutte, L., De Prijck, S., Deswarte, K., Malissen, B., Hammad, H., and Lambrecht, B.N. (2013). Alveolar macrophages develop from fetal monocytes that differentiate into long-lived cells in the first week of life via GM-CSF. J. Exp. Med. *210*, 1977–1992. https://doi.org/10.1084/jem.20131199.
3. Schneider, C., Nobs, S.P., Kurrer, M., Rehrauer, H., Thiele, C., and Kopf, M. (2014). Induction of the nuclear receptor PPAR-γ by the cytokine GM-CSF is critical for the differentiation of fetal monocytes into alveolar macrophages. Nat. Immunol. *15*, 1026–1037. https://doi.org/10.1038/ni.3005.
4. Evren, E., Ringqvist, E., and Willinger, T. (2020). Origin and ontogeny of lung macrophages: from mice to humans. Immunology *160*, 126–138. https://doi.org/10.1111/imm.13154.
5. Wculek, S.K., Heras-Murillo, I., Mastrangelo, A., Mañanes, D., Galán, M., Miguel, V., Curtabbi, A., Barbas, C., Chandel, N.S., Enríquez, J.A., et al. (2023). Oxidative phosphorylation selectively orchestrates tissue macrophage homeostasis. Immunity *56*, 516–530.e9. https://doi.org/10.1016/j.immuni.2023.01.011.
6. Fujii, W., Kapellos, T.S., Baßler, K., Händler, K., Holsten, L., Knoll, R., Warnat-Herresthal, S., Oestreich, M., Hinkley, E.R., Hasenauer, J., et al. (2021). Alveolar macrophage transcriptomic profiling in COPD shows major lipid metabolism changes. ERJ Open Res. *7*, 100915. https://doi.org/10.1183/23120541.00915-2020.
7. Robb, L., Drinkwater, C.C., Metcalf, D., Li, R., Köntgen, F., Nicola, N.A., and Begley, C.G. (1995). Hematopoietic and lung abnormalities in mice with a null mutation of the common beta subunit of the receptors for granulocyte-macrophage colony-stimulating factor and interleukins 3 and 5. Proc. Natl. Acad. Sci. *92*, 9565–9569. https://doi.org/10.1073/pnas.92.21.9565.
8. Stanley, E., Lieschke, G.J., Grail, D., Metcalf, D., Hodgson, G., Gall, J.A., Maher, D.W., Cebon, J., Sinickas, V., and Dunn, A.R. (1994). Granulocyte/macrophage colony-stimulating factor-deficient mice show no major perturbation of hematopoiesis but develop a characteristic pulmonary pathology. Proc. Natl. Acad. Sci. USA *91*, 5592–5596. https://doi.org/10.1073/pnas.91.12.5592.
9. Gao, X., Zhu, B., Wu, Y., Li, C., Zhou, X., Tang, J., and Sun, J. (2022). TFAM-Dependent Mitochondrial Metabolism Is Required for Alveolar Macrophage Maintenance and Homeostasis. J. Immunol. *208*, 1456–1466. https://doi.org/10.4049/jimmunol.2100741.
10. Izquierdo, H.M., Brandi, P., Gómez, M.-J., Conde-Garrosa, R., Priego, E., Enamorado, M., Martínez-Cano, S., Sánchez, I., Conejero, L., Jimenez-Carretero, D., et al. (2018). Von Hippel-Lindau Protein Is Required for Optimal Alveolar Macrophage Terminal Differentiation, Self-Renewal, and Function. Cell Rep. *24*, 1738–1746. https://doi.org/10.1016/j.celrep.2018.07.034.
11. Iliopoulos, O., Levy, A.P., Jiang, C., Kaelin, W.G., and Goldberg, M.A. (1996). Negative regulation of hypoxia-inducible genes by the von Hippel-Lindau protein. Proc. Natl. Acad. Sci. *93*, 10595–10599. https://doi.org/10.1073/pnas.93.20.10595.
12. Maxwell, P.H., Wiesener, M.S., Chang, G.-W., Clifford, S.C., Vaux, E.C., Cockman, M.E., Wykoff, C.C., Pugh, C.W., Maher, E.R., and Ratcliffe, P.J. (1999). The tumour suppressor protein VHL targets hypoxia-inducible factors for oxygen-dependent proteolysis. Nature *399*, 271–275. https://doi.org/10.1038/20459.
13. Stebbins, C.E., Kaelin, W.G., and Pavletich, N.P. (1999). Structure of the VHL-ElonginC-ElonginB complex: implications for VHL tumor suppressor function. Science *284*, 455–461. https://doi.org/10.1126/science.284.5413.455.
14. Kaelin, W.G. (2022). Von Hippel–Lindau disease: insights into oxygen sensing, protein degradation, and cancer. J. Clin. Investig. *132*, e162480. https://doi.org/10.1172/JCI162480.
15. Wang, G.L., Jiang, B.H., Rue, E.A., and Semenza, G.L. (1995). Hypoxia-inducible factor 1 is a basic-helix-loop-helix-PAS heterodimer regulated by cellular O2 tension. Proc. Natl. Acad. Sci. *92*, 5510–5514. https://doi.org/10.1073/pnas.92.12.5510.
16. Koh, M.Y., and Powis, G. (2012). Passing the baton: the HIF switch. Trends Biochem. Sci. *37*, 364–372. https://doi.org/10.1016/j.tibs.2012.06.004.
17. Yang, S.-L., Wu, C., Xiong, Z.-F., and Fang, X. (2015). Progress on hypoxia-inducible factor-3: Its structure, gene regulation and biological function (Review). Mol. Med. Rep. *12*, 2411–2416. https://doi.org/10.3892/mmr.2015.3689.
18. Hu, L., Xie, H., Liu, X., Potjewyd, F., James, L.I., Wilkerson, E.M., Herring, L.E., Xie, L., Chen, X., Cabrera, J.C., et al. (2020). TBK1 Is a Synthetic Lethal Target in Cancer with *VHL* Loss. Cancer Discov. *10*, 460–475. https://doi.org/10.1158/2159-8290.CD-19-0837.
19. Frew, I.J., and Krek, W. (2008). pVHL: A Multipurpose Adaptor Protein. Sci. Signal. *1*, pe30. https://doi.org/10.1126/scisignal.124pe30.
20. Ji, Q., and Burk, R.D. (2008). Downregulation of integrins by von Hippel-Lindau (VHL) tumor suppressor protein is independent of VHL-directed hypoxia-inducible factor alpha degradation. Biochem. Cell. Biol. *86*, 227–234. https://doi.org/10.1139/O08-035.
21. Yang, H., Minamishima, Y.A., Yan, Q., Schlisio, S., Ebert, B.L., Zhang, X., Zhang, L., Kim, W.Y., Olumi, A.F., and Kaelin, W.G. (2007). pVHL Acts as an Adaptor to Promote the Inhibitory Phosphorylation of the NF-κB Agonist Card9 by CK2. Mol. Cell *28*, 15–27. https://doi.org/10.1016/j.molcel.2007.09.010.
22. Hergovich, A., Lisztwan, J., Barry, R., Ballschmieter, P., and Krek, W. (2003). Regulation of microtubule stability by the von Hippel-Lindau tumour suppressor protein pVHL. Nat. Cell Biol. *5*, 64–70. https://doi.org/10.1038/ncb899.
23. Li, S., Li, W., Yuan, J., Bullova, P., Wu, J., Zhang, X., Liu, Y., Plescher, M., Rodriguez, J., Bedoya-Reina, O.C., et al. (2022). Impaired oxygen-sensitive regulation of mitochondrial biogenesis within the von Hippel–Lindau syndrome. Nat. Metab. *4*, 739–758. https://doi.org/10.1038/s42255-022-00593-x.
24. Briston, T., Stephen, J.M., Thomas, L.W., Esposito, C., Chung, Y.-L., Syafruddin, S.E., Turmaine, M., Maddalena, L.A., Greef, B., Szabadkai, G., et al. (2018). VHL-Mediated Regulation of CHCHD4 and Mitochondrial Function. Front. Oncol. *8*, 388. https://doi.org/10.3389/fonc.2018.00388.
25. Zhu, S., Ding, W., Chen, Y., Wang, W., Xu, R., Liu, C., Liu, X., and Deng, H. (2022). High *VHL* Expression Reverses Warburg Phenotype and Enhances Immunogenicity in Kidney Tumor Cells. Genom. Proteom. Bioinform. *20*, 657–669. https://doi.org/10.1016/j.gpb.2019.12.002.
26. Zhang, W., Li, Q., Li, D., Li, J., Aki, D., and Liu, Y.-C. (2018). The E3 ligase VHL controls alveolar macrophage function via metabolic–epigenetic regulation. J. Exp. Med. *215*, 3180–3193. https://doi.org/10.1084/jem.20181211.
27. Jaśkiewicz, M., Moszyńska, A., Króliczewski, J., Cabaj, A., Bartoszewska, S., Charzyńska, A., Gebert, M., Dąbrowski, M., Collawn, J.F., and Bartoszewski, R. (2022). The transition from HIF-1 to HIF-2 during prolonged hypoxia results from reactivation of PHDs and HIF1A mRNA instability. Cell. Mol. Biol. Lett. *27*, 109. https://doi.org/10.1186/s11658-022-00408-7.
28. Dengler, V.L., Galbraith, M., and Espinosa, J.M. (2014). Transcriptional regulation by hypoxia inducible factors. Crit. Rev. Biochem. Mol. Biol. *49*, 1–15. https://doi.org/10.3109/10409238.2013.838205.
29. Gautier, E.L., Shay, T., Miller, J., Greter, M., Jakubzick, C., Ivanov, S., Helft, J., Chow, A., Elpek, K.G., Gordonov, S., et al. (2012). Gene-expression profiles and transcriptional regulatory pathways that underlie the

identity and diversity of mouse tissue macrophages. Nat. Immunol. *13*, 1118–1128. https://doi.org/10.1038/ni.2419.

30. van de Laar, L., Saelens, W., De Prijck, S., Martens, L., Scott, C.L., Van Isterdael, G., Hoffmann, E., Beyaert, R., Saeys, Y., Lambrecht, B.N., and Guilliams, M. (2016). Yolk Sac Macrophages, Fetal Liver, and Adult Monocytes Can Colonize an Empty Niche and Develop into Functional Tissue-Resident Macrophages. Immunity *44*, 755–768. https://doi.org/10.1016/j.immuni.2016.02.017.

31. Huang, X., Cao, M., and Xiao, Y. (2023). Alveolar macrophages in pulmonary alveolar proteinosis: origin, function, and therapeutic strategies. Front. Immunol. *14*, 1195988. https://doi.org/10.3389/fimmu.2023.1195988.

32. Crucet, M., Wüst, S.J.A., Spielmann, P., Lüscher, T.F., Wenger, R.H., and Matter, C.M. (2013). Hypoxia enhances lipid uptake in macrophages: role of the scavenger receptors Lox1, SRA, and CD36. Atherosclerosis *229*, 110–117. https://doi.org/10.1016/j.atherosclerosis.2013.04.034.

33. Nath, B., Levin, I., Csak, T., Petrasek, J., Mueller, C., Kodys, K., Catalano, D., Mandrekar, P., and Szabo, G. (2011). Hepatocyte-specific hypoxia-inducible factor-1α is a determinant of lipid accumulation and liver injury in alcohol-induced steatosis in mice. Hepatol. Baltim. Md *53*, 1526–1537. https://doi.org/10.1002/hep.24256.

34. Parathath, S., Mick, S.L., Feig, J.E., Joaquin, V., Grauer, L., Habiel, D.M., Gassmann, M., Gardner, L.B., and Fisher, E.A. (2011). Hypoxia is present in murine atherosclerotic plaques and has multiple adverse effects on macrophage lipid metabolism. Circ. Res. *109*, 1141–1152. https://doi.org/10.1161/CIRCRESAHA.111.246363.

35. Cramer, T., Yamanishi, Y., Clausen, B.E., Forster, I., Pawlinski, R., Mackman, N., Haase, V.H., Jaenisch, R., Corr, M., Nizet, V., et al. (2003). HIF-1 alpha is essential for myeloid cell-mediated inflammation. Cell *113*, 419.

36. Matak, P., Heinis, M., Mathieu, J.R.R., Corriden, R., Cuvellier, S., Delga, S., Mounier, R., Rouquette, A., Raymond, J., Lamarque, D., et al. (2015). Myeloid HIF-1 is protective in Helicobacter pylori-mediated gastritis. J. Immunol. *194*, 3259–3266. https://doi.org/10.4049/jimmunol.1401260.

37. Palsson-McDermott, E.M., Curtis, A.M., Goel, G., Lauterbach, M.A.R., Sheedy, F.J., Gleeson, L.E., van den Bosch, M.W.M., Quinn, S.R., Domingo-Fernandez, R., Johnston, D.G.W., et al. (2015). Pyruvate Kinase M2 Regulates Hif-1α Activity and IL-1β Induction and Is a Critical Determinant of the Warburg Effect in LPS-Activated Macrophages. Cell Metab. *21*, 65–80. https://doi.org/10.1016/j.cmet.2014.12.005.

38. Peyssonnaux, C., Datta, V., Cramer, T., Doedens, A., Theodorakis, E.A., Gallo, R.L., Hurtado-Ziola, N., Nizet, V., and Johnson, R.S. (2005). HIF-1α expression regulates the bactericidal capacity of phagocytes. J. Clin. Investig. *115*, 1806–1815. https://doi.org/10.1172/JCI23865.

39. Tannahill, G.M., Curtis, A.M., Adamik, J., Palsson-McDermott, E.M., McGettrick, A.F., Goel, G., Frezza, C., Bernard, N.J., Kelly, B., Foley, N.H., et al. (2013). Succinate is an inflammatory signal that induces IL-1β through HIF-1α. Nature *496*, 238–242. https://doi.org/10.1038/nature11986.

40. Schaible, B., Schaffer, K., and Taylor, C.T. (2010). Hypoxia, innate immunity and infection in the lung. Respir. Physiol. Neurobiol. *174*, 235–243. https://doi.org/10.1016/j.resp.2010.08.006.

41. Traylor, Z.P., Aeffner, F., and Davis, I.C. (2013). Influenza A H1N1 induces declines in alveolar gas exchange in mice consistent with rapid post-infection progression from acute lung injury to ARDS. Influenza Other Respir. Viruses *7*, 472–479. https://doi.org/10.1111/j.1750-2659.2012.00414.x.

42. Woods, P.S., Kimmig, L.M., Sun, K.A., Meliton, A.Y., Shamaa, O.R., Tian, Y., Cetin-Atalay, R., Sharp, W.W., Hamanaka, R.B., and Mutlu, G.M. (2022). HIF-1α induces glycolytic reprograming in tissue-resident alveolar macrophages to promote cell survival during acute lung injury. eLife *11*, e77457. https://doi.org/10.7554/eLife.77457.

43. Aki, D., Li, Q., Li, H., Liu, Y.-C., and Lee, J.H. (2019). Immune regulation by protein ubiquitination: roles of the E3 ligases VHL and Itch. Protein Cell *10*, 395–404. https://doi.org/10.1007/s13238-018-0586-8.

44. Zhu, B., Wu, Y., Huang, S., Zhang, R., Son, Y.M., Li, C., Cheon, I.S., Gao, X., Wang, M., Chen, Y., et al. (2021). Uncoupling of macrophage inflammation from self-renewal modulates host recovery from respiratory viral infection. Immunity *54*, 1200–1218.e9. https://doi.org/10.1016/j.immuni.2021.04.001.

45. Imtiyaz, H.Z., Williams, E.P., Hickey, M.M., Patel, S.A., Durham, A.C., Yuan, L.-J., Hammond, R., Gimotty, P.A., Keith, B., and Simon, M.C. (2010). Hypoxia-inducible factor 2alpha regulates macrophage function in mouse models of acute and tumor inflammation. J. Clin. Investig. *120*, 2699–2714. https://doi.org/10.1172/JCI39506.

46. Rankin, E.B., Rha, J., Selak, M.A., Unger, T.L., Keith, B., Liu, Q., and Haase, V.H. (2009). Hypoxia-inducible factor 2 regulates hepatic lipid metabolism. Mol. Cell Biol. *29*, 4527–4538. https://doi.org/10.1128/MCB.00200-09.

47. Liu, Y., Ma, Z., Zhao, C., Wang, Y., Wu, G., Xiao, J., McClain, C.J., Li, X., and Feng, W. (2014). HIF-1α and HIF-2α are critically involved in hypoxia-induced lipid accumulation in hepatocytes through reducing PGC-1α-mediated fatty acid β-oxidation. Toxicol. Lett. *226*, 117–123. https://doi.org/10.1016/j.toxlet.2014.01.033.

48. Wood, E.G., Macdougall, C.E., Blythe, H., Clément, M., Colas, R.A., Dalli, J., Marelli-Berg, F., and Longhi, M.P. (2020). HIF1α activation in dendritic cells under sterile conditions promotes an anti-inflammatory phenotype through accumulation of intracellular lipids. Sci. Rep. *10*, 20825. https://doi.org/10.1038/s41598-020-77793-6.

49. Gainullina, A., Mogilenko, D.A., Huang, L.-H., Todorov, H., Narang, V., Kim, K.-W., Yng, L.S., Kent, A., Jia, B., Seddu, K., et al. (2023). Network analysis of large-scale ImmGen and Tabula Muris datasets highlights metabolic diversity of tissue mononuclear phagocytes. Cell Rep. *42*, 112046. https://doi.org/10.1016/j.celrep.2023.112046.

50. Caton, M.L., Smith-Raska, M.R., and Reizis, B. (2007). Notch–RBP-J signaling controls the homeostasis of CD8− dendritic cells in the spleen. J. Exp. Med. *204*, 1653–1664. https://doi.org/10.1084/jem.20062648.

51. Menendez-Montes, I., Escobar, B., Palacios, B., Gómez, M.J., Izquierdo-Garcia, J.L., Flores, L., Jiménez-Borreguero, L.J., Aragones, J., Ruiz-Cabello, J., Torres, M., and Martin-Puig, S. (2016). Myocardial VHL-HIF Signaling Controls an Embryonic Metabolic Switch Essential for Cardiac Maturation. Dev. Cell *39*, 724–739. https://doi.org/10.1016/j.devcel.2016.11.012.

52. Haase, V.H., Glickman, J.N., Socolovsky, M., and Jaenisch, R. (2001). Vascular tumors in livers with targeted inactivation of the von Hippel–Lindau tumor suppressor. Proc. Natl. Acad. Sci. *98*, 1583–1588. https://doi.org/10.1073/pnas.98.4.1583.

53. Ryan, H.E., Poloni, M., McNulty, W., Elson, D., Gassmann, M., Arbeit, J.M., and Johnson, R.S. (2000). Hypoxia-inducible factor-1alpha is a positive factor in solid tumor growth. Cancer Res. *60*, 4010–4015.

54. Albendea-Gomez, T., Mendoza-Tamajon, S., Castro-Mecinas, R., Escobar, B., Ferreira Rocha, S., Urra-Balduz, S., Nicolas-Avila, J.A., Oliver, E., Villalba-Orero, M., and Martin-Puig, S. (2025). Vascular HIF2 Signaling Prevents Cardiomegaly, Alveolar Congestion, and Capillary Remodeling During Chronic Hypoxia. Arterioscler. Thromb. Vasc. Biol. *45*, e78–e98. https://doi.org/10.1161/ATVBAHA.124.321780.

55. Gruber, M., Hu, C.-J., Johnson, R.S., Brown, E.J., Keith, B., and Simon, M.C. (2007). Acute postnatal ablation of Hif-2alpha results in anemia. Proc. Natl. Acad. Sci. USA *104*, 2301–2306. https://doi.org/10.1073/pnas.0608382104.

56. The R Core Team (2019). R: A Language and Environment for Statistical Computing (R Foundation for Statistical Computing) Version 4.2.1. .

57. Manso, B.A., and Medina, K.L. (2021). Standardized flow-cytometry-based protocol to simultaneously measure transcription factor levels. STAR Protoc. *2*, 100485. https://doi.org/10.1016/j.xpro.2021.100485.

58. Love, M.I., Huber, W., and Anders, S. (2014). Moderated estimation of fold change and dispersion for RNA-seq data with DESeq2. Genome Biol. *15*, 550. https://doi.org/10.1186/s13059-014-0550-8.

59. Korotkevich, G., Sukhov, V., Budin, N., Shpak, B., Artyomov, M.N., and Sergushichev, A. (2016). Fast gene set enrichment analysis. Preprint at Bioinformatics. https://doi.org/10.1101/060012.

60. Alexey Sergushichev (2017). Fgsea (Bioconductor). https://doi.org/10.18129/B9.BIOC.FGSEA.

61. Carvalho, B.S., and Irizarry, R.A. (2010). A framework for oligonucleotide microarray preprocessing. Bioinformatics *26*, 2363–2367. https://doi.org/10.1093/bioinformatics/btq431.

62. Ritchie, M.E., Phipson, B., Wu, D., Hu, Y., Law, C.W., Shi, W., and Smyth, G.K. (2015). limma powers differential expression analyses for RNA-sequencing and microarray studies. Nucleic Acids Res. *43*, e47. https://doi.org/10.1093/nar/gkv007.

63. Phipson, B., Lee, S., Majewski, I.J., Alexander, W.S., and Smyth, G.K. (2016). Robust hyperparameter estimation protects against hypervariable genes and improves power to detect differential expression. Ann. Appl. Stat. *10*, 946–963. https://doi.org/10.1214/16-AOAS920.

64. Yu, G., Wang, L.-G., Han, Y., and He, Q.-Y. (2012). clusterProfiler: an R Package for Comparing Biological Themes Among Gene Clusters. OMICS A J. Integr. Biol. *16*, 284–287. https://doi.org/10.1089/omi.2011.0118.

## STAR★METHODS

### KEY RESOURCES TABLE

| REAGENT or RESOURCE | SOURCE | IDENTIFIER |
|---|---|---|
| Antibodies | | |
| anti-CD16/CD32 (clone 2.4G2) | Cytek Biosciences | Cat# 70–0161, RRID: AB_2621487 |
| anti-CD11c-BV 510 (clone HL3) | BD | Cat# 562949, RRID: AB_2732056 |
| anti-CD11c – APC/Fire (clone N418) | BioLegend | Cat# 117352, RRID: AB_2572124 |
| anti-Siglec-F - PE (clone E50-2440) | BD | Cat# 552126, RRID: AB_394341 |
| anti-CD64 - A647 (clone X54-5/7.1) | BD | Cat# 558539, RRID: AB_647120 |
| anti-CD11b - PE/Cy7 (clone M1/70) | BD | Cat# 552850, RRID: AB_394491 |
| anti-F4/80 - FITC (clone BM8) | Life Technologies | Cat# 11-4801-82, RRID: AB_2637191 |
| anti-I-A/I-E-FITC (clone 2G9) | BD | Cat# 553623, RRID: AB_394958 |
| anti-I-A/I-E – APC (clone M5/114.15.2) | Tonbo Biosciences | Cat# 20–5321, RRID: AB_2621603 |
| anti-Ly6G - APC (clone 1A8) | BD | Cat# 560599, RRID: AB_1727560 |
| anti-Ly6G - PE (clone 1A8) | BD | Cat# 551461, RRID: AB_394208 |
| anti-Ly6C - FITC (clone AL21) | BD | Cat# 553104, RRID: AB_394628 |
| anti-CD45 - PE (clone 30-F11) | eBioscience | Cat# 12-0451-82, RRID: AB_465668 |
| anti-CD45.1 – PE (clone A20) | BD | Cat# 553776, RRID: AB_395044 |
| anti-CD45.1 – APC/Fire 750 (clone A20) | BioLegend | Cat# 110752, RRID: AB_2629806 |
| anti-CD45.2 – APC (clone 104) | BD | Cat# 558702, RRID: AB_1645215 |
| anti-Ki67 – eFluor 660 (clone SolA15) | eBioscience | Cat# 50-5698-80, RRID: AB_2574234 |
| anti-Rat IgG2aκ isotype control (clone eBR2a) | eBioscience | Cat# 50-4321-80, RRID: AB_10598640 |
| anti-BrdU - APC (from BD kit) | BD | Cat# 552598, RRID: AB_2861367 |
| anti-CD11c – BV421 (clone HL3) | BD | Cat# 562782, RRID: AB_2737789 |
| anti-Siglec-F – FITC (clone S17007L) | BioLegend | Cat# 155503, RRID: AB_2750232 |
| anti-HIF-1α (clone D2U3T) | Cell Signaling | Cat# 14179S, RRID: AB_2622225 |
| anti-HIF-2α (clone E2N9W) | Cell Signaling | Cat# 57921S, RRID: AB_2942106 |
| anti-Rabbit IgG – Alexa Fluor 594 | Thermo Fisher | Cat# A-21207, RRID: AB_141637 |
| Mouse CD11c MicroBeads UltraPure | Miltenyi | Cat# 130-125-835, RRID: AB_3750744 |
| Chemicals, peptides, and recombinant proteins | | |
| Ghost Dye® Red 780, Viability Dye | Cytek | SKU# 13-0865-T100 |
| Pentobarbital sodium, 200 mg/mL (Dolethal) | Vetoquinol | CN: 570681.8 |
| Ketamine 100 mg/mL (Imalgene) | Boehringer Ingelheim | CN: 579557 |
| Xylazine Hydrochloride 20 mg/mL (Rompun) | Elanco Animal Health Gmbh | CN: 572126 |
| Medetomidine hydrochloride 1 mg/mL (Medeson) | Industrial Veterinaria S.A. | CN: 573212 |
| Red Blood Cell Lysing Buffer Hybri-Max™ | Merck | Sku# R7757-100ML |
| Mouse GM-CSF, Animal-Free Recombinant Protein | ThermoFisher/PeproTech® | Cat# AF-315-03-20UG |
| Corning® Cell-Tak™ Cell and Tissue Adhesive | Corning | Cat# 354241 |
| Oligomycin A | Sigma-Aldrich | Cat# O4876-5MG |
| Carbonyl cyanide 3-chlorophenylhydrazone (CCCP) | Sigma-Aldrich | Cat# C2759-1G |
| Rotenone | Sigma-Aldrich | Cat# R8875-1G |

(*Continued on next page*)

*Continued*

| REAGENT or RESOURCE | SOURCE | IDENTIFIER |
|---|---|---|
| Antimycin A | Sigma-Aldrich | Cat# A8674-50MG |
| 16% Formaldehyde Solution (w/v) Methanol-free | ThermoFisher | Cat# 28908 |
| L-Carnitine hydrochloride | Sigma-Aldrich | Cat# C0283-5G |
| Palmitoyl coenzyme A lithium sal | Sigma-Aldrich | Cat# P9716-5MG |
| **Critical commercial assays** | | |
| BD Pharmingen™ APC BrDU Kit | BD | Cat# 557892 |
| eBioscience™ Foxp3/Transcription Factor Staining Buffer Kit | ThermoFisher | Cat# 00-5523-00 |
| Foxp3/Transcription Factor Staining Buffer Kit | Cytek | SKU# TNB-0607-KIT |
| Seahorse XFe96 FluxPak | Agilent | 102416–100 |
| RNeasy Micro Kit | Qiagen | Cat# 74004 |
| Pierce™ BCA Protein Assay Kit | ThermoFisher | Cat# 23225 |
| Mouse SP-D DuoSet ELISA | R&D Systems | Cat# DY6839-05 |
| **Deposited data** | | |
| Microarray Affymetrix Mouse Gene 1.1 ST Array of Adult AMs and postnatal day 2 AMs | Schneider et al.[3] | GEO: GSE60249 |
| RNA-seq of CD11cΔ*Vhl* macrophages | Izquierdo et al.[10] | GEO: GSE108975 |
| RNA-seq of CD11cΔ*Vhl*Δ*Hif1a*, CD11cΔ*Vhl*Δ*Hif2a*, CD11cΔ*Vhl*Δ*Hif1a*Δ*Hif2a* macrophages | This paper | GEO: GSE325293 |
| **Experimental models: Organisms/strains** | | |
| CD11c-Cre mice: B6.Cg-Tg(Itgax-cre)1-1Reiz/J | Donated by B. Reizis[50] | RRID:IMSR_JAX:008068 |
| *Vhl*$^{fl/fl}$mice: C;129S-*Vhl*$^{tm1Jae}$/J | Donated by S. Martin-Puig,[51] generated by Haase et al.[52] | RRID:IMSR_JAX:004081 |
| *Hif1a*$^{f/f}$ mice: B6.129-*Hif1a*$^{tm3Rsjo}$/J | Donated by S. Martin-Puig,[51] generated by Ryan et al.[53] | RRID:IMSR_JAX:007561 |
| *Hif2a*$^{fl/fl}$ mice: STOCK *Epas1*$^{tm1Mcs}$/J | Donated by S. Martin-Puig,[54] generated by Gruber et al.[55] | RRID:IMSR_JAX:008407 |
| *Csf2rb*$^{-/-}$ mice: B6.129S1-*Csf2rb*$^{tm1Cgb}$/J | Donated by M. Guilliams, generated by Robb et al.[7] | RRID:IMSR_JAX:005940 |
| CD45.2$^{+}$ mice: C57BL/6JOlaHsd | Harlan, Inotiv | MGI ID MGI:216418 |
| CD45.1$^{+}$ mice: B6.SJL-*Ptprc*$^{a}$ *Pepc*$^{b}$/BoyJ | The Jackson Laboratory | RRID:IMSR_JAX:002014 |
| **Oligonucleotides** | | |
| A list of qPCR primers can be found in Table S1 | This paper | N/A |
| **Software and algorithms** | | |
| R v4.2.1 | R Core team[56] | https://www.R-project.org/ |
| DESeq2 (v1.36.0) | Bioconductor | https://doi.org/10.1186/s13059-014-0550-8 |
| Sva (3.44.0) | Bioconductor | https://doi.org/10.18129/B9.bioc.sva |
| GOSemSim (v2.22.0) | Bioconductor | https://doi.org/10.18129/B9.bioc.GOSemSim |
| oligo R package (v1.71.7) | Bioconductor | https://doi.org/10.18129/B9.bioc.oligo |
| limma R package (v3.64.3) | Bioconductor | https://doi.org/10.18129/B9.bioc.limma |
| clusterProfiler (v4.16.0) | Bioconductor | https://doi.org/10.18129/B9.bioc.clusterProfiler |
| Triwise R package (v0.99.5) | Github | https://github.com/saeyslab/triwise |

(*Continued on next page*)

*Continued*

| REAGENT or RESOURCE | SOURCE | IDENTIFIER |
|---|---|---|
| Fgsea R package (1.22.0) | Bioconductor | https://doi.org/10.18129/B9.bioc.fgsea |
| GraphPad Prism 10.4.1 | GraphPad | N/A |
| FlowJo v10.8.1 | Becton, Dickinson and Company | N/A |
| Other | | |
| 18 G x 1 1/2 in. BD™ blunt fill needle (bronchoalveolar lavages) | BD | SKU# 305180 |
| MS positive selection columns | Miltenyi Biotec | Cat# 130-042-201 |

## EXPERIMENTAL MODEL AND STUDY PARTICIPANT DETAILS

### Animal models

Mice colonies were bred at Centro Nacional de Investigaciones Cardiovasculares Carlos III (CNIC) under specific pathogen-free conditions. Experiments were conducted with 8- to 10-weeks-old age-matched littermates (regardless of gender). Floxed *Vhl* mice[52] were backcrossed with or without floxed *Hif1a*[53] and floxed *Hif2a*,[55] provided by Silvia Martin-Puig (IIBM, Madrid, Spain).[51,54] Additionally, all possible combinations were backcrossed with CD11c-Cre mice (B6.Cg-Tg(*Itgax*-cre)1-1Reiz/J), kindly provided by Boris Reizis (New York University Grossman School of Medicine, New York)[50] in order to allow the targeting of the alveolar macrophage compartment. *Csf2rb*$^{-/-}$ mice, kindly provided by Martin Guilliams,[7] and F1 from the mating between C57BL/6J mice expressing the CD45.2 allele (Harlan, Inotiv) and B6/SJL (Ptprca Pepcb/BoyJ) mice expressing the CD45.1 allele were also used. All experimental procedures were approved by the institutional care and use committees and conformed to EU Directive 2010/63EU and Recommendation 2007/526/EC regarding the protection of animals used for experimental and other scientific purposes, enforced in Spanish law under Royal Decree 53/2013.

## METHOD DETAILS

### AM isolation

Mice were sacrificed with a lethal dose of pentobarbital (Dolethal, Vetoquinol). To isolate AMs for cell culture, ten bronchoalveolar lavages (BAL) were done by inserting a venal catheter (18G BD Pharmingen) into the trachea with 1ml of phosphate-buffered saline (PBS), 5 mM EDTA, and 2% inactivated fetal bovine serum (FBS, Sigma-Aldrich) (FACS buffer) at 37°C. Samples were kept on ice until further processing. BAL was centrifuged at 300 G for 10′ at 4°C and red blood cell lysis was performed at room temperature (RT) for 3 min with RBC Lysis Buffer (Sigma-Aldrich). Cells were resuspended in medium or FACs buffer depending on the application.

### AM *in vitro* culture

AMs from BAL were cultured in RPMI 1640 (Gibco) supplemented with 10% FBS, 100 U/ml Penicillin and Streptomycin (Lonza), 1mM Sodium Pyruvate (HyClone™), and 2 mM L-glutamine (complete RPMI) at 37°C and 5% $CO_2$. For *in vitro* proliferation assay, cells were supplemented with 10 pg/ml rGM-CSF (Peprotech). AMs were pulsed twice with BrdU (BD Pharmingen) at 10μM: 10-12 h and 24h after culture onset. 24h after the second pulse, cells were washed once with PBS to remove remaining FBS and incubated with accutase (StemCell Technologies) for 15-20′ at 37°C. Cells were carefully detached by pipetting. After centrifugation at 600 G for 5′ at 4°C, cells were resuspended and counted, and the same cell number per condition and genotype was stained for surface markers and BrdU.

### Flow cytometry

Single-cell suspensions were stained in 96-U-bottom plates. Surface staining was performed in FACS buffer: PBS, 2.5 mM EDTA and 2.5% heat-inactivated FBS (iFBS). Staining was performed for 15-20′ at 4°C with FcR block anti-mouse CD16/CD32 (2.4G2, Cytek) and the appropriate mix of the following fluorochrome-conjugated antibodies in FACS buffer: CD11c (clone HL3, BD Biosciences or clone N418, Biolegend), Siglec-F (clone E50-2440, BD Biosciences), CD64 (clone X54-5/7.1, BD Biosciences), CD11b (clone M1/70, BD Biosciences), F4/80 (clone BM8, Life Technologies), MHCII (clone M5/114.15.2, Cytek), Ly6G (clone 1A8, BD), Ly6C (clone AL21, BD Biosciences), CD45 (30-F11, eBiosciences), CD45.1 (A20, eBiosciences and Biolegend), CD45.2 (clone 104, BD Biosciences). Hoechst 33258 (Invitrogen) or Ghost Dye Red 780 (Cytek) were used as a counterstain to exclude dead cells. For intracellular Ki67 staining, AMs were stained for surface markers as described above, washed twice with FACs buffer at 600 G for 5′ at 4°C, and mixed with unstained thymocytes, used as a cell carrier. Fixation and permeabilization of cells were performed using the Foxp3/Transcription Factor Staining Buffer Set (Cat# 00-5523-00, Invitrogen) and following manufacturer's instructions. Briefly, fixation solution was prepared by diluting Fixation/Permeabilization concentrate, 1:3 with Fixation/Perm diluent. Permeabilization buffer 10x was diluted 1:10 with sterile water and kept on ice (Perm buffer). Cells were fixed for 30′ at 4°C in the dark. Cells were washed with Perm buffer and intracellular (i.c.) staining was done right after. Intracellular staining with anti-Ki67-eFluor 660 (SolA15, eBiosciences)

or isotype control Rat IgG2aκ (eBR2a, eBiosciences) was performed in Perm buffer. All centrifugations after fixation were done at 1000 G for 5′ at 4°C. Cells were resuspended in FACS buffer before acquisition. Intracellular BrdU staining was done following manufacturer instructions. In brief, AMs were stained and mixed with carrier cells as above-mentioned and fixed and permeabilized using the BrdU staining set (BD Pharmingen). Cells were treated with DNAse and stained with anti-BrdU Ab (BD Pharmingen). For intracellular HIF-1α and HIF-2α staining, AMs were stained for surface markers with BV421 Hamster anti-mouse CD11c (BD, clone HL3) and FITC Rat anti-mouse Siglec-F (Biolegend, clone S17007L) and Ghost Dye Red 780 (Cytek) as described above. Cells were washed twice with FACS buffer at 600 G for 5′ at 4°C. Cells were then fixed using the Foxp3/Transcription Factor Staining Buffer Kit (Cytek, SKU TNB-0607-KIT), using freshly prepared 1x Fix/Perm solution for 20 minutes at 4°C. Cells were then washed twice with 200 μL of FACS buffer (all centrifugations at 1000 G, 4°C, 5 minutes after fixation). Cells were permeabilized with 100 μL of 1x freshly prepared Foxp3 Permeabilization buffer 1x (Perm buffer) from the same kit and then resuspended in diluted antibody solution (HIF-1α or HIF-2α) plus FcR block anti-mouse CD16/CD32 (2.4G2, Tonbo Biosciences) prepared in Perm buffer. HIF-1α (Clone D2U3T Rabbit, Cell Signaling cat. # 14179S) and HIF-2α (Clone E2N9W Rabbit, Cell Signaling cat. # 57921S) were used at 1:50 dilution, and FcR block was used at 1:200 dilution. Cells were stained for 45 minutes at RT, and then washed three times with 200 μL of Perm buffer. Next, secondary antibody staining was performed at 1:500 dilution of Donkey anti-Rabbit IgG, Alexa Fluor™ 594 secondary antibody (ThermoFisher, Cat.# A-21207) in Perm buffer plus FcR block (1:200), for 30 minutes at RT. Samples kept in parallel that had been stained with surface markers but not with intracellular antibodies were stained with secondary antibody alone as control. Cells were washed again three times and resuspended in FACS buffer for sample acquisition. Quantification of HIF transcription factor levels was calculated as in Manso et al.[57] Briefly: background staining was subtracted as described to calculate specific expression level: HIF Stain gMFI – Secondary antibody alone gMFI. Samples were acquired in SP6800 Spectral, LSRFortessa, or FACSymphony cell analyzers, and data was analyzed using FlowJo Version 10 software.

### Real-time oxygen consumption rate and glycolytic flux

Real-time oxygen consumption rate (OCR) and extracellular acidification rate (ECAR) were determined with Seahorse XF-96 Extracellular Flux Analyzer (Agilent Technologies). AMs from fresh BAL were pooled from 5-10 mice per genotype. After red blood cell lysis, $2.5x10^5$ AMs were plated in Cell-Tak (Corning) coated wells. The assay was performed in DMEM supplemented with 100 μg/ml penicillin, 100 μg/ml streptomycin, and either 25 mM glucose, 1 mM pyruvate, and 2 mM glutamine or 5 mM L-carnitine and 50 μM palmitoyl-CoA (all Sigma). pH was adjusted to 7.4 with KOH. Three consecutive measurements were performed under basal conditions and after the sequential addition of the following inhibitors: 1 μM Oligomycin, 1 μM Carbonyl cyanide 3-chlorophenylhydrazone (CCCP), and 1 μM Rotenone with 1 μM Antimycin A. Basal respiratory rate (BRR), maximal respiratory rate (MRR), spare respiratory capacity (SRC) and basal ECAR were calculated according to Seahorse Agilent indications.

### RNA sequencing and analysis

CD11c cell positive selection was performed on BAL suspensions from 3-5 mice per genotype. Mouse CD11c MicroBeads UltraPure and MS columns (all Miltenyi Biotec) were used according to manufacturers' instructions. Briefly, cells were resuspended in 100 μL of FACS buffer plus 20 μL of CD11c MicroBeads and incubated on ice for 30 mins. Then, cells were washed and purified by magnetic positive selection with MS columns (Miltenyi). A total of 3 pools of 3-5 mice per genotype were included. Total RNA was isolated using Rneasy Micro Kit (Qiagen), and RNA quality was validated with a 2100 Bioanalyzer (Agilent). RNA sequencing was performed in the Genomics Unit of the CNIC on Illumina HiSeq 2500 System. Sequencing reads were pre-processed through a pipeline that used FastQC to assess read quality and Cutadapt to trim sequencing reads, eliminate Illumina adaptor remains, and discard reads that were shorter than 30 base pairs. The resulting reads were mapped against the mouse transcriptome (GRCm38.99) with STAR. Expected expressions were quantified using RSEM, and batch normalization was applied with Combat as implemented in the sva (v3.44.0) R package. Genes were filtered to have at least 10 CPM, and data were normalized using the trimmed mean of m values (TMM) method, both with edgeR (v3.38.4). DESeq2 rlog-normalized values[58] were used to generate Hexagonal Triwise diagrAMs with Triwise package. Significantly different genes for each pair-wise comparison (adj. $p$-value < 0.05, logFC > 1.5) are displayed as red dots in the plots. Genes were ranked according to log-Fold change, and gene set enrichment analysis was performed using the FGSEA (v1.22.0) R package[59,60] along with the Kyoto Encyclopedia of Genes and Genomes (KEGG) (www.genome.jp/kegg) and Gene Ontology (GO) (www.geneontology.org/) databases. Redundant GO terms were removed using the GOSemSim R package. Heatmaps display deregulated genes (Adj. $p$-value $\leq$ 0.05) of the specified gene sets.

For PCA-based enrichment analysis, $\log_2$(CPM) samples were scaled and used as input for principal component analysis (PCA). Genes were ranked according to the loading vectors of PC1. Resulting ranks were used as input for the FGSEA R package along with the KEGG and GO databases in order to identify the main sources of variability detected by PCA. Only gene sets with a number of genes $\geq$ 15 and $\leq$ 500 were considered for PCA-based enrichment analysis.

### Analysis of public GSE60249 microarray data and over-representation analysis

Array data (CEL files) from Schneider et al.[3] stored under accession number GSE60249 were downloaded from GEO. Import, quality control and normalization was performed with the oligo R package[61] (v1.71.7). The array annotation database mogene11sttranscriptcluster.db was used to map expression values with their associated Ensembl gene IDs. Differential expression analysis was calculated using limma[62,63] (v3.64.3).

For over-representation analysis (ORA), the intersect between genes significantly upregulated in P2 vs adult macrophages from GSE60249 (adj. $p$-value < 0.05, logFC > 0) and genes significantly upregulated in our datasets (adj. $p$-value < 0.05, logFC > 0) was selected. Then, ORA was performed using clusterProfiler[64] (v4.16.0) along with the KEGG database.

### Bone marrow transfer mixed chimeras

B6/SJL mice expressing the CD45.1 congenic marker were lethally irradiated with 2 doses of 6 Gy that were 3 h apart and reconstituted intravenously with $5x10^6$ cells of a 1:1 mixture of $CD45.1^+$ $CD45.2^+$ wild-type BM cells and $CD45.2^+$ BM cells coming from the indicated experimental genotypes. Mice were analyzed 45-50 days after reconstitution as previously described. A small sample of peripheral blood was harvested one day before the experimental endpoint to test immune compartment reconstitution.

### Pulmonary macrophage transplantation

$5x10^4$ $A10^4$ A Ms from BAL were transferred intratracheally into $Csf2rb^{-/-}$ mice. Recipient mice were anesthetized with Ketamine (Imalgene, Boehringer Ingelheim) and Xylazine (Rompun, Elanco Animal Health Gmbh). When entirely unconscious, a small incision was made to partially expose the trachea. Then, mice were carefully intubated orotracheally with an IV catheter (22 G; BD Insyte). Cells were inoculated with a pipette in 30µl of PBS. Next, mice were extubated, and the incision sutured. Mice were finally injected with anesthesia reversor (Medeson, Industrial Veterinaria S.A.) and kept in a warm plaque until complete recovery. 1ml PBS1x-BAL from recipient mice was collected six weeks after transplantation. Cells were centrifuged at 1700 rpm for 5 min at RT and supernatant was used to measure total protein concentration by BCA (Pierce BCA Protein Assay Kit, Thermo Scientific) and surfactant protein D (SP-D) concentration by ELISA (SP-D DUO ELISA kit, R&D Systems), according to the manufacturer's instruction. Cell engraftment was compared by flow cytometry of total lung cells.

## QUANTIFICATION AND STATISTICAL ANALYSIS

Statistical comparisons were analyzed using R v.4.2.1 or GraphPad Prism v10.4.1. Data are presented as individual values and were analyzed as indicated in the legends or the dedicated methods section. All experiments were repeated at least twice, and pooled data from several experiments are shown as indicated in the legends. All $n$ values represent biological replicates (different mice, primary cell preparations, or *in vitro* experiments). Differences were considered significant when $p < 0.05$ and are indicated as *ns* when not significant, $^*p < 0.05$, $^{**}p < 0.01$, $^{***}p < 0.001$, $^{****}p < 0.0001$.